






## Strong Long-Lived Anticyclonic Mesoscale Eddies in the Balearic Sea: Formation, Intensification, and Thermal Impact

E. Aguiar<sup>1</sup> , B. Mourre<sup>1</sup> , A. Alvera-Azcárate<sup>2</sup>, A. Pascual<sup>3</sup> , E. Mason<sup>3</sup> , and J. Tintoré<sup>1,3</sup> 

<sup>1</sup>SOCIB, Palma de Mallorca, Spain, <sup>2</sup>University of Liege, Liege, Belgium, <sup>3</sup>IMEDEA (UIB-CSIC), Esporles, Spain

### Key Points:

- Northwesterly (NW) wind events and the existence of the Pyrenees thermal front are both necessary for the formation of strong long-lived Balearic Sea eddies
- Eddy intensification was driven by salinity gradients in 2010 and by additional NW wind events in 2017
- Both events created long-lasting surface temperature anomalies that have the characteristics of local marine heatwaves

### Supporting Information:

Supporting Information may be found in the online version of this article.

### Correspondence to:

E. Aguiar and B. Mourre,  
[eguiar@socib.es](mailto:eguiar@socib.es);  
[bmourre@socib.es](mailto:bmourre@socib.es)

### Citation:

Aguiar, E., Mourre, B., Alvera-Azcárate, A., Pascual, A., Mason, E., & Tintoré, J. (2022). Strong long-lived anticyclonic mesoscale eddies in the Balearic Sea: Formation, intensification, and thermal impact. *Journal of Geophysical Research: Oceans*, 127, e2021JC017589. <https://doi.org/10.1029/2021JC017589>

Received 16 JUN 2021  
 Accepted 24 APR 2022

**Abstract** Anticyclonic mesoscale eddies are often observed in the Balearic Sea (BS) toward the end of summer and autumn. In some years, these eddies become strong and persistent, modifying the local water mass properties. In this study, we analyze two of the most significant recent long-lived anticyclonic eddies, occurring in 2010 and 2017, using data from a high-resolution circulation model, altimetry and satellite-borne sea surface temperature observations. These eddies lasted around 2 and 4 months, respectively, with a radius varying between 40 and 75 km. The generation and intensification mechanisms of these long-lived anticyclonic eddies are studied by means of (a) energy conversion terms associated with eddy-mean flow interaction and (b) model sensitivity tests. Results show that these eddies were formed and intensified through mixed barotropic and baroclinic instabilities. The former are produced under the action of intense northwesterly (NW) winds. The latter are related to the existence of an intense summer thermal front between the BS and the Gulf of Lion, and to northward inflows of relatively lower salinity waters. Both the wind events and the presence of the thermal front are necessary for the formation of the eddies. The intensification process varied between both events. While in 2010 it was driven by significant salinity gradients produced by northwards inflows, in 2017 it was produced by additional intense NW winds. Both long-lived anticyclonic eddies created long-lasting surface temperature anomalies up to 2.5°C, which have characteristics of local marine heatwaves.

**Plain Language Summary** Eddies are closed circular currents present in the oceans. They are important phenomena due to their capacity to isolate water masses, retain floating particles and modify ocean circulation. In the Western Mediterranean Sea there is a recognized area of anticyclonic eddy presence between Barcelona and the Balearic Islands, especially during late summer. Specifically, in 2010 and 2017 two such eddies were identified with lifetimes of 2 and 4 months, respectively. In this paper, we investigate why these eddies were so long and persistent in comparison with other years. Results confirm that these eddies are generated as a result of northwesterly (NW) winds events blowing over an area with two water masses of different temperature. In 2010, low salinity northward water inflows sustained this eddy during two months, while in 2017 the eddy remained active for a period of four months under the influence of additional intense NW winds. Both eddies created long-lasting surface temperature anomalies, in particular in 2017, the sea surface temperature within the eddy influence area was 2.5°C warmer in comparison to other years.

## 1. Introduction

Mesoscale eddies are one of the most energetic forms of flow in the ocean (Chelton, Schlax, & Samelson, 2011; Ferrari & Wunsch, 2009) with important implications for ocean dynamics. Eddy-transport influence biogeochemical cycles through the redistribution of heat, salt, carbon and nutrients (Chelton, Gaube, et al., 2011; Dong et al., 2014; Gaube et al., 2014; Gaube & McGillicuddy, 2017; Kahru et al., 2007; Mahadevan & Archer, 2000; Nagai et al., 2015; Siegel et al., 2011; Wang et al., 2018; Zhang et al., 2014). Moreover, eddy-mean flow interaction produces exchanges of energy and momentum that can induce changes in the general ocean circulation (Fox-Kemper et al., 2019; Greatbatch, 1987; Hogg & Stommel, 1985; Holland, 1978; Holland & Lin, 1975; Marshall, 2006). Mesoscale eddies can have time scales of days to months and spatial scales of tens to hundreds of kilometers. The exchanges and transports produced by eddies are highly dependent on their life cycle and on their structure (Capet et al., 2014; d'Ovidio et al., 2013; Rypina et al., 2020). The study of the evolution of these eddies, as well as their generation and intensification mechanisms is essential to better understand these exchanges. Eddies can trap water masses of different origin producing local temperature and/or salinity anomalies, which may have important implications on oceanic ecosystems and climate. Eddies also play an important role in the dispersion or retention of pollutants (Brach et al., 2018), plankton species (Condie & Condie, 2016; Krom et al., 1992; Salihoğlu et al., 1990; Taupier-Letage et al., 2003) and larvae (Lobel & Robinson, 1986; Sabaté

© 2022. The Authors.

This is an open access article under the terms of the [Creative Commons Attribution-NonCommercial-NoDerivs License](https://creativecommons.org/licenses/by/4.0/), which permits use and distribution in any medium, provided the original work is properly cited, the use is non-commercial and no modifications or adaptations are made.

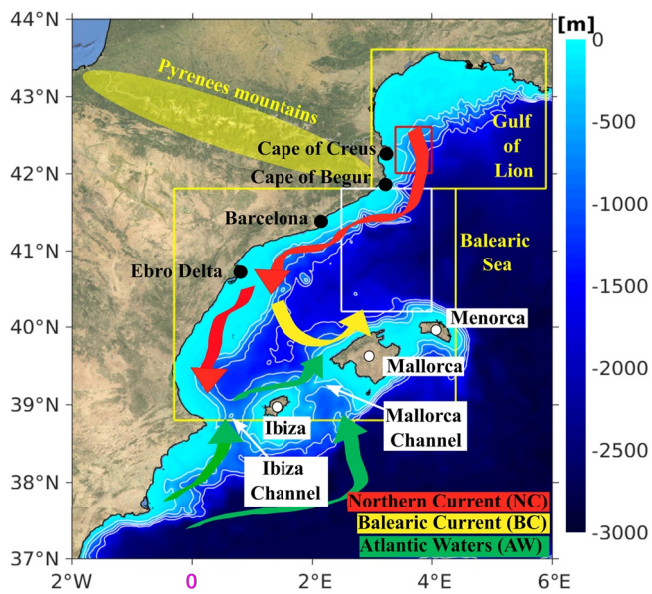


**Figure 1.** Main oceanographic features in the study area: Northern and Balearic currents. Green arrows denote waters of recent Atlantic origin that occasionally flow northward through the Ibiza and Mallorca Channels. The boundaries of the Balearic Sea and the Gulf of Lions are marked by yellow lines. White box represents the eddy-influence area. The red box indicates the area considered for the northwesterly winds analysis. Bathymetric contours are depicted for 300, 700, 1100 and 1500 m depth levels.

et al., 2007, 2013), as well as on the behavior of different species such as, for example, turtles (Gaube et al., 2017) and/or sharks (Gaube et al., 2018).

The BS, which is located in the Western Mediterranean Sea (WMS, Figure 1) is an area characterized by the presence of intense mesoscale anticyclonic eddies regularly observed south of Cape of Begur (Font et al., 1988; Garreau et al., 2011; Onken et al., 2008; Pascual et al., 2002; Rubio et al., 2005, 2009; Tintoré et al., 1990) during late summer and autumn (Mason & Pascual, 2013). The Rossby radius of deformation is around 10 km in this area (Escudier et al., 2016), which is one third to one half of typical value for the Atlantic and Pacific Ocean at the same latitude (Chelton et al., 1998).

While these anticyclonic eddies usually disappear after a few weeks, some of them remain in the same area for more than 1 month, becoming “long-lived” eddies (Escudier et al., 2016). Based on the analysis of satellite altimeter data, Aguiar et al. (2019) identified three of these long-lived anticyclonic eddies in 1998, 2010 and 2017. These eddies were characterized as being strong based on their large sea surface height (SSH) signature, which in turn implies high values of eddy kinetic energy (EKE). In the Mediterranean Sea, the EKE is commonly used to characterize mesoscale eddies (e.g., Amitai et al., 2010; Pessini et al., 2018; Poulain et al., 2012; Pujol & Larnicol, 2005). The presence of long-lived mesoscale features in this area is of high importance since it is located in the path of the Northern Current (NC), which is a main feature of the whole Mediterranean Sea circulation. Their presence deviates the NC toward the ocean interior, creating a blocking effect associated with favorable conditions for northward inflows through the Ibiza Channel (IC) in the southern part. Here we use high-resolution model simulations to further understand the associated formation and intensification mechanisms.

The accepted paradigm for the mechanisms of eddy generation suggests that they are mainly produced through ocean current instability (Pedlosky, 1982). The instabilities can be barotropic, due to horizontal current shear (often related to the dynamical interaction of the winds with currents); and/or baroclinic due to the vertical shear of the currents associated with the tilting of isopycnal surfaces. In the BS, even though several studies have discussed the mechanisms of eddy generation, no consensus has yet been reached. Based on repeated hydrographic data, Font et al. (1988) proposed that cyclonic eddies could be generated by baroclinic instability mechanisms. Analyzing observations from a field study carried out in July 1983, Tintoré et al. (1990) suggested that their formation was related to the spreading of fresh water from the Gulf of Lions that interacts with the local bathymetry. Pascual et al. (2002), based on a description of satellite images and hydrographic data in 1998, proposed that the presence of relatively warm waters from recent Atlantic origin in the BS combined with NW wind shear downstream of the Pyrenees mountains were the main factors for the generation of the eddies. Investigating the eddy observed in 2001 by Rubio et al. (2005) and using model sensitivity tests and energy transfer analysis from a simulation of ocean conditions during the summer 2002, Rubio et al. (2009) related the generation of the eddy to the coastal flow separation next to Cape of Creus under the effect of an intense NW wind event. The eddy was then found to be advected southwards into the BS. Garreau et al. (2011) studied the long-lived eddy observed in autumn 2007 through numerical modeling and in situ observations and argued that the eddies in the BS were linked to eddies produced farther north, in an area of accumulation of potential energy found in the southwestern part of the Gulf of Lion, under the effects of NW winds, leading to the isolation of a warm and low-density dense water body in the BS. Notice that Hu et al. (2011) identified strong NW winds and stratification as necessary conditions for the formation of these anticyclonic eddies in the western part of the Gulf of Lion north of the BS.

While the previous studies in the BS analyzed the formation of eddies identified in specific years, both short- and long-lived, an interannual perspective using both numerical simulations and observations is necessary to better understand not only the process of eddy formation but also their intensification. The present study fills this gap by analyzing and comparing the mechanisms of eddy formation and intensification of the two most energetic

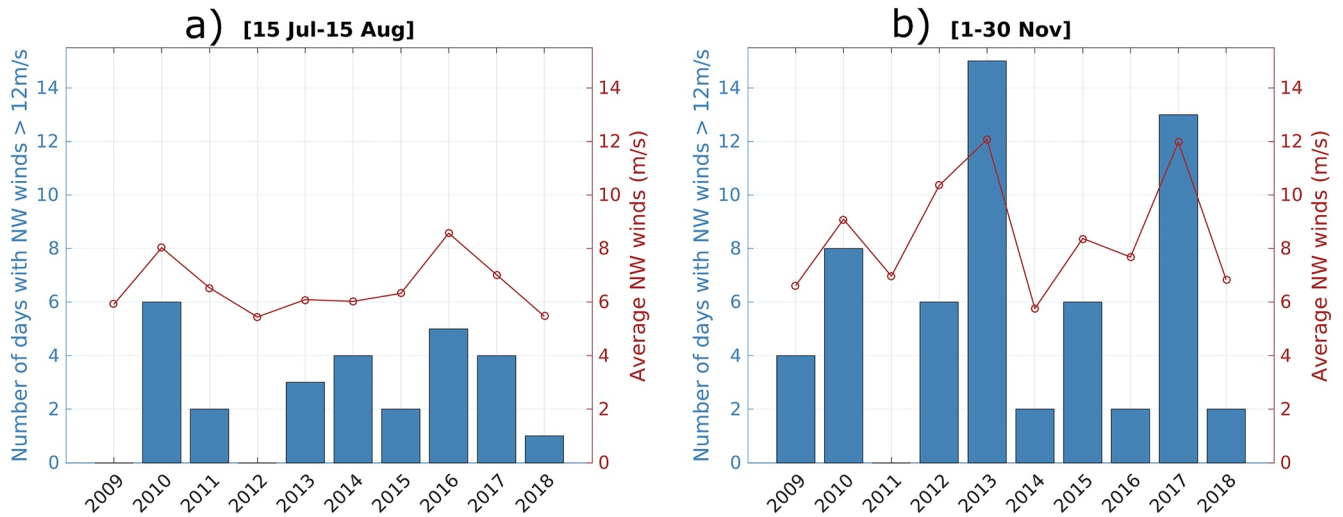


**Figure 2.** Interannual variability over the 2009–2018 period of intense Northwesterly (NW) winds extracted within the red box represented in Figure 1, (a) from 15 July to 15 August and (b) from 1 to 30 November. The bars represent the number of days with average NW winds intensities higher than 12 m/s and the red line denotes the average-intensity of the NW winds. Data come from the high-resolution HIRLAM wind model fields used to force the Western Mediterranean Operational Modelling System ocean model and provided by the Spanish Meteorological Agency.

long-lived anticyclonic eddy events over the last 20 years. In addition, the effects of these long-lived anticyclonic eddies are also analyzed here in terms of their associated thermal anomaly.

Numerical models are valuable tools to analyze the details of the generation and growth of intense long-lived eddies. We use a high-resolution ( $\sim 2$  km) inter-annual free-run simulation that allows the spontaneous generation and further intensification of these mesoscale eddies (see Section 2.2 for more details). The model provides a complete description of the evolution of the eddy allowing us to investigate the generation and intensification mechanisms by means of (a) energy conversion terms associated with eddy-mean flow interaction and (b) model sensitivity tests to relate the simulated variability of eddies with external forcings. The first method, as used in previous studies in other regions of the world (e.g., Beckmann et al., 1994; Jouanno et al., 2009; Kang & Curchitser, 2015; Zhan et al., 2016), provides a characterization of the spatial patterns of the energy conversion terms and a quantification of the energy transfer rates associated with barotropic and baroclinic instabilities. The second allows us to identify more explicitly the drivers of this variability, as also done by Rubio et al., 2009 with a focus on wind and Rhône river forcings.

The paper is organized as follows: the study area, numerical simulation, observations, and methodology are described in Section 2. Section 3 characterizes the two long-lived anticyclonic eddies examined in this study based on altimetry data and model outputs. The main mechanisms involved in the generation and intensification of the eddies are evaluated in Section 4, by means of the study of the model eddy-mean flow energy terms and their spatio-temporal variability throughout the eddy lifetimes, complemented by model sensitivity experiments to identify the main drivers. Finally, the discussion in Section 5 provides an overall synthesis of the results, offers scenarios to explain the generation and intensification of these eddies, and explores their thermal impact.

## 2. Materials and Methods

### 2.1. Study Area

The Balearic Sea (BS, Figure 1) is bordered at the north by the Gulf of Lion and at the south by the Ibiza and Mallorca channels. The BS dynamics are characterized by a strong boundary current (the so-called NC, NC) flowing southwestward along the Iberian Peninsula slope (Font et al., 1988; Millot, 1999) until it splits into two branches at approximately  $40.6^\circ\text{N}$ : one flows southward through the IC and the other turns cyclonically and forms part of the Balearic Current (BC; Millot&Taupier-Letage, 2005). The area is characterized by the occurrence of intense NW wind events that blow from southern France into the Gulf of Lion and BS Jansà, (1987). The cold and dry nature of these winds induces surface evaporation and cooling. Figure 2 describes the interannual

variability over the period 2009–2018 of these intense NW winds during two periods associated with the formation and intensification of the long-lived anticyclonic eddies respectively, that is, (a) from 15 July to 15 August and (b) from 1 to 30 November. During the formation period, the 3 years with the largest numbers of days with NW winds over 12 m/s and the largest average NW wind intensities are 2010, 2016 and 2017. During the November period, 2013 and 2017 present a remarkable high number of days with intense NW winds, also resulting in higher average NW wind intensities.

During summer, the surface layer is locally warmer within the BS than in the Gulf of Lion due to differential heating and mixing produced by the shadow effect of the Pyrenees Mountains on the NW winds (López-García et al., 1994). As a result, an intense surface thermal front is generated perpendicular to the coast at  $\sim 42^\circ\text{N}$ , known as the Pyrenees Front (López-García et al., 1994; Pascual et al., 2002).

The southern channels are characterized by the presence of strong meridional salinity gradients, due their favorable conditions for the intrusion of low-salinity waters of recent Atlantic origin from the southern sub-basin (Barceló-Llull et al., 2019; Heslop et al., 2012; Juza et al., 2019; Mason & Pascual, 2013). Specifically, in the Mallorca channel the values of the surface salinity are maximum/minimum in spring/autumn (Barceló-Llull et al., 2019).

## 2.2. Model Simulation

The Balearic Islands Coastal Observing and Forecasting System (SOCIB, Tintoré et al., 2013, 2019) generates high-resolution numerical simulations based on the Western Mediterranean Operational Modeling System (WMOP, Juza et al., 2016; Mourre et al., 2018). Western Mediterranean Operational Modelling System is based on a regional configuration of the Regional Ocean Modeling System ROMS (Shchepetkin & McWilliams, 2005) with a horizontal resolution of around 2 km. The WMOP hindcast simulation used in this study (Aguiar et al., 2020; Mourre et al., 2018) is nested in the larger-scale  $1/16^\circ$  (6–7 km) Mediterranean Reanalysis simulation of the Copernicus Marine Service (CMEMS, Simoncelli et al., 2019). It uses 32 sigma-levels resulting in a vertical resolution varying from 1 to 2 m at the surface, 30–40 m at 200 m depth and around 250 m at 1000 m depth. The WMOP simulation uses atmospheric forcing from the high-resolution (3 h–5 km) HIRLAM model from the Spanish Meteorological Agency AEMET (Undén et al., 2002). The simulation includes observed daily river discharges from the six major rivers of the domain (Var, Rhône, Aude, Hérault, Ebro and Júcar) over the period 2009–2018 provided by the French HYDRO database and the Spanish hydrographic confederations for the Ebro and Júcar rivers.

In this work, we use a free-run inter-annual simulation spanning the period 2009–2018, which has been exhaustively validated using multi-platform observational data from the coastal to the sub-basin scale. Aguiar et al. (2020) showed that this free-run simulation produced an improvement of the mean surface circulation within the BS in comparison with its parent model. It was also shown to reproduce realistic eddy statistics at the scales observed by altimetry. The eddy activity of this simulation was also assessed by Mourre et al. (2018), showing realistic patterns and magnitude of EKE in comparison with altimetry, after spatial and temporal filtering to remove the impact of the small spatiotemporal scales that are not resolved by the satellite products.

## 2.3. Observations

### 2.3.1. Satellite Altimetry

The sea level daily gridded datasets from satellite observations are used to detect strong long-lived eddies over the 1993–2018 period by means of the spatially averaged EKE, sea level anomaly (SLA) and surface relative vorticity time series within the eddy-influence area (Section 3.1). These datasets are interpolated onto a  $1/8^\circ$  spatial resolution grid (around 12 km) over the Mediterranean region and distributed by CMEMS and referenced as SEALEVEL\_MED\_PHY\_L4\_REP\_OBSERVATIONS\_008\_051. This product is created by the SL-TAC multi-mission altimeter data processing system, using data from all available altimeter missions. Data are interpolated at crossover locations and dates, and then cross-validated, filtered for residual noise and small-scale signals, and sub-sampled. Finally, an optimal interpolation is applied in order to compute interpolated SLA by merging data from all the satellites.



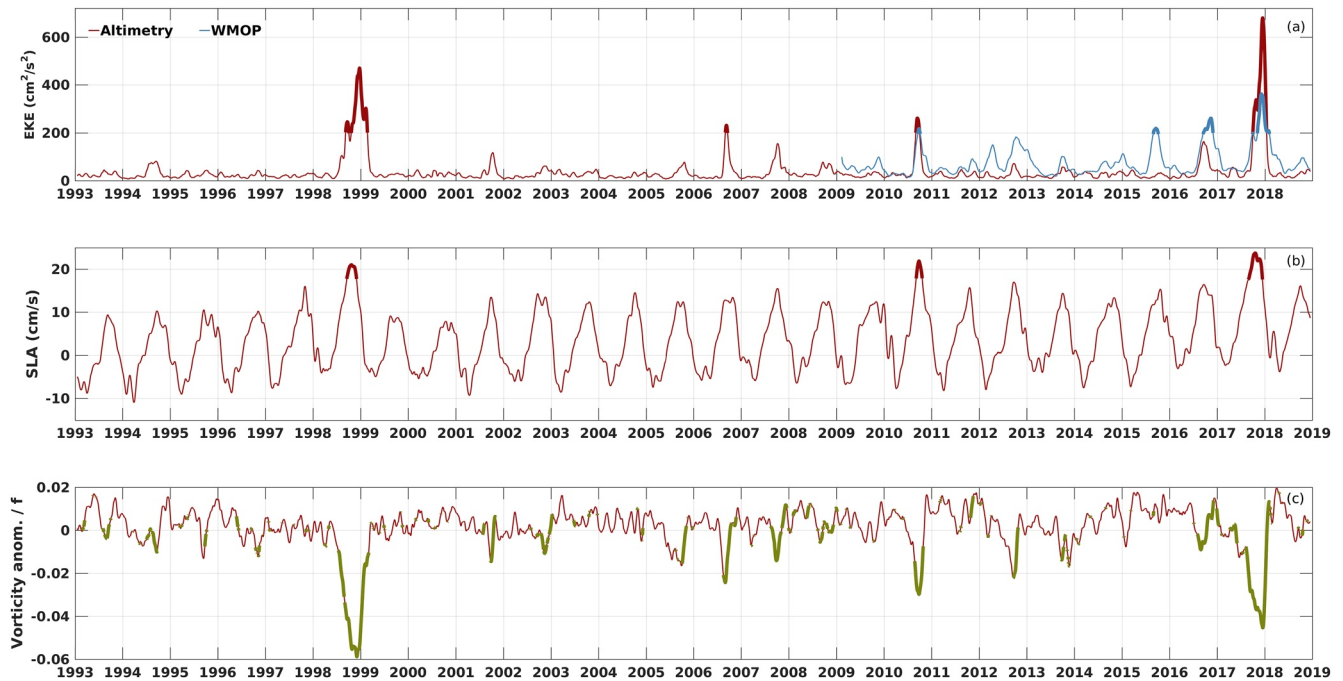


**Figure 3.** (a) Temporally filtered (30-day moving average) and spatially averaged eddy kinetic energy (EKE) from altimetry and spatially filtered Western Mediterranean Operational Modeling System fields over the eddy-influence area depicted in Figure 1 [2.5°–4°E; 40.2°–41.8°N]; (b) same for altimeter sea level anomaly (SLA), and (c) same for altimeter-derived scaled surface relative vorticity anomaly superimposed with the OW-based eddy identification. The thick lines in (a) and (b) denote values higher than the mean plus two standard deviations of altimeter EKE or SLA 2009–2018 time series. The green line in (c) represents periods with identification of eddies according to the OW detection criterion.

The EKE is quantified as  $\frac{1}{2} (u_{ga}^2 + v_{ga}^2)$ , where the geostrophic velocities  $u_{ga}$  and  $v_{ga}$  are derived from the SLA field through the equation for geostrophic equilibrium. The scaled surface relative vorticity anomaly is computed as  $\frac{1}{f} \left( \frac{\partial v_{ga}}{\partial x} - \frac{\partial u_{ga}}{\partial y} \right)$ , where  $f$  denotes the Coriolis parameter ( $f = 2\Omega \sin \lambda$ ,  $\Omega$ : rotation of the Earth,  $\lambda$ : latitude of the study area).

### 2.3.2. Satellite Sea Surface Temperature

Satellite sea surface temperature (SST) observations are used to evaluate the thermal impact of the eddies. In the framework of CMEMS, different remotely sensed SST products are produced operationally and distributed in near-real time by the Instituto di Scienze dell'Atmosfera e del Clima – Gruppo di Oceanografia da Satellite (ISAC-GOS). The ISAC-GOS processing chain modules are described by Buongiorno Nardelli et al. (2013). The product used in this work is referenced as SST\_MED\_SSTA\_L4\_NRT\_OBSERVATIONS\_010\_004 and has a resolution of 1/16° (~7–8 km).

### 2.4. Eddy-Mean Flow Interaction: Theoretical Framework

In this work, we are specifically interested in the origin of the EKE and how it is transferred from other forms of available energy, so as to improve our understanding of the generation and intensification mechanisms of eddies.

From a simplified and theoretical point of view, the energy reservoirs within a fixed ocean domain are: the mean flow kinetic energy (MKE), the EKE, the mean flow potential energy (MPE) and the eddy potential energy (EPE; Kang & Curchitser, 2015; Storch et al., 2012; Xie et al., 2007; Figure 3). Energy transfer between these reservoirs occurs by means of eddy-mean flow interaction through barotropic and/or baroclinic instability. These energy transfer terms are considered following the framework described in Beckmann et al. (1994) and represented by Equations 1–3:

$$T_2 = -\frac{g^2}{\rho_0 N^2} \iiint \overline{u' \rho'} \cdot \left( \frac{\partial \bar{\rho}}{\partial x} \right) + \overline{v' \rho'} \cdot \left( \frac{\partial \bar{\rho}}{\partial y} \right) dV \quad (1)$$

$$T_3 = -g \cdot \iiint \overline{\rho' w'} dV \quad (2)$$

$$T_4 = -\rho_0 \cdot \iiint \overline{u'u'} \cdot \left( \frac{\partial \bar{u}}{\partial x} \right) + \overline{u'v'} \cdot \left( \frac{\partial \bar{v}}{\partial x} + \frac{\partial \bar{u}}{\partial y} \right) + \overline{v'v'} \cdot \left( \frac{\partial \bar{v}}{\partial y} \right) dV \quad (3)$$

Where  $\rho_0 = 1025 \text{ kg m}^{-3}$  is the background density of seawater,  $\rho$  is the density and  $u, v, w$  the zonal, meridional and vertical components of the velocity field, and the overbars denote time averages. The eddy energy can be obtained from the mean flow through barotropic (T4 term: MKE  $\rightarrow$  EKE) and/or baroclinic instability (T2 term: MPE  $\rightarrow$  EPE). EKE can be in turn received from the EPE (T3 term: EPE  $\rightarrow$  EKE). Positive values of T2 and T4 imply mean-to-eddy energy conversions and positive values of T3 conversions from eddy potential to kinetic energy. Both T2 and T3 describe energy conversion associated with baroclinic instability. T2 is related to horizontal density gradients and T3 to vertical movements of water masses. T2 is the conversion between MPE and EPE, and it is commonly interpreted as an indication of baroclinic instability processes. However, these processes also need a transfer from EPE to EKE, which is given by T3. So, following Jouanno et al. (2009) we consider the generation of EKE through baroclinic instability processes when both terms are found to be positive.

The examination of these energy conversion terms has been widely used to study the dominant mechanisms of eddy generation, such as in Capó et al. (2018) in the Mediterranean Sea, Beckmann et al. (1994) in the North Atlantic Ocean, Jouanno et al. (2009) in the Caribbean Sea, Kang & Curchitser (2015) in the Gulf Stream region or Zhan et al. (2016) in the Red Sea.

### 2.5. Okubo-Weiss Eddy Detection Method

The presence or absence of eddies is assessed by means of the Okubo-Weiss detection method (OW, Okubo, 1970; Weiss, 1991) based on the relationship between vorticity and strain. This method identifies eddies as regions where vorticity (rotation) dominates over strain (deformation). The OW parameter is defined as,  $OW = S_n^2 + S_s^2 - W^2$  where  $S_n = \frac{\partial u_g}{\partial x} - \frac{\partial v_g}{\partial y}$  is the normal strain,  $S_s = \frac{\partial v_g}{\partial x} + \frac{\partial u_g}{\partial y}$  the shear strain and  $W = \frac{\partial v_g}{\partial x} - \frac{\partial u_g}{\partial y}$  the relative vorticity. A specific threshold (OWo) of minus two spatial standard deviations of the OW values is defined to identify eddies, as in Isern-Fontanet et al. (2004). Eddies are identified when OW values are lower than OWo.

## 3. Identification and Evolution of Long-Lived Eddies in the BS

### 3.1. Strong Long-Lived Eddies Over the 1993–2018 Period

Figure 3 depicts the time series of altimeter EKE, SLA and surface relative vorticity anomaly spatially averaged over the eddy-influence area represented in Figure 1 [2.5°–4°E; 40.2°–41.8°N]. The presence of eddy as identified by the OW criterion is superimposed in the time series of relative vorticity. Moreover, the equivalent WMOP model surface geostrophic EKE time series is also displayed together with the altimeter EKE. All signals were also low-pass filtered using a 30-day moving average to detect only long-lived eddies longer than one month, following the definition given by Escudier et al. (2016). Model geostrophic velocities used to compute the WMOP model EKE were previously spatially filtered (32 km spatial moving average) to remove the small-scale spatial variability that is not reproduced by altimetry maps (Ballarotta et al., 2019). The thick lines in panels (a) and (b) highlight the values higher than the mean plus two standard deviations of altimeter EKE or SLA time series over the common period with the model simulation (2009–2018). The value of this threshold is  $43.2 + 2 \cdot 77.2 = 197.6 \text{ cm}^2/\text{s}^2$  for EKE time series and  $3.4 + 2 \cdot 7.1 = 17.6 \text{ cm}$  for SLA time series. In panel (c), the green lines indicate the presence of eddies according the OW criterion.

Strong long-lived anticyclonic eddies are identified as those events that (a) exceed the two standard deviation threshold for both EKE and SLA, and (b) are detected by the O-W method coinciding with negative values of the relative vorticity anomaly.

According to this procedure, three strong long-lived anticyclonic eddies are identified during the 26-year time series: in 1998, 2010 and 2017. All of them occur in late summer and/or autumn. The strongest peaks of EKE were reached in 1998 and 2017, with values above  $450 \text{ cm}^2/\text{s}^2$  and  $680 \text{ cm}^2/\text{s}^2$  respectively. These high values of EKE are comparable to the maximum values reached in the most energetic areas of the Mediterranean Sea (Pujol and Larnicol, 2005) such as the Alboran Gyres showing values larger than  $600 \text{ cm}^2/\text{s}^2$  (Juza et al., 2016b), the Algerian basin (maxima around  $350 \text{ cm}^2/\text{s}^2$ , Pessini et al., 2018) and the Ierapetra Eddy with maximum EKE over  $500 \text{ cm}^2/\text{s}^2$  (Amitai et al., 2010).

The duration of the long-lived anticyclonic eddies is given by the mean plus one standard deviation of the altimeter EKE time series ( $43.2 + 77.2 = 123.4 \text{ cm}^2/\text{s}^2$ ). The WMOP EKE time-series, starting in 2009, correctly reproduces the 2010 and 2017 eddies as two of the most intense anticyclonic eddies in the 2009–2018 period. Note that the 1998 eddy, which is the longest event of the time series (182 days, from 30 August 1998–28 February 1999), was previously reported and studied by Pascual et al. (2002). The 2001 and 2007 eddies observed by Rubio et al. (2005) and Garreau et al. (2011), respectively, are also visible in the altimetry EKE time series (Figure 3a) and detected by the OW method (Figure 3c). However, in terms of intensity, these eddies remained under the  $2\sigma$  threshold for both EKE and SLA (Figure 3b). **Notice also that the 2002 eddy investigated by means of a numerical simulation in Rubio et al. (2009) only generates a very moderate signal in the time series.**

The model also identifies two other long-lived anticyclonic eddies in 2015 and 2016. While no eddy was detected in altimetry in 2015, a relatively intense eddy was also observed in 2016, but was just below the threshold defined here for strong long-lived eddies.

The 2017 eddy is the most intense with a peak around  $680 \text{ cm}^2/\text{s}^2$  in altimetry. The filtered model represents a smaller peak intensity ( $\text{EKE}_{\text{WMOP}} = 350 \text{ cm}^2/\text{s}^2$ ) but a longer lasting eddy spanning 166 days from 06 September 2017 to 19 February 2018, versus 117 days in altimetry (22 September 2017–17 January 2018).

The 2010 eddy is shorter and less intense than the 2017 eddy: it lasts 51 days in the model (29 August 2010–19 October 2010) versus 49 days in altimetry (22 August 2010–10 October 2010), with peaks at  $209 \text{ cm}^2/\text{s}^2$  and  $262 \text{ cm}^2/\text{s}^2$  for the model and altimetry, respectively, showing a good overall agreement between model and altimetry for this eddy.

### 3.2. Monthly Evolution of the 2010 and 2017 Long-Lived Eddies in Model and Altimetry Sea Level Anomalies

Figure 4 shows a comparison between monthly averaged SLA from altimetry and WMOP, from August to November in 2010 (Figure 4a) and from August 2017 to January 2018 (Figure 4b). The anomalies have been computed with respect to the time average sea level over the periods 1993–2012 for altimetry and 2009–2018 for the model. Moreover, the spatial mean has been removed to obtain zero-centered fields in both cases.

In 2010 (Figure 4a), the eddy generated by the model has a similar lifetime as the eddy observed by altimetry, although the exact shape and temporal evolution of the simulated eddy differs from the observations. The WMOP simulation produces an eddy that remains near the coast during the entire event, while altimetry data shows a southeastward displacement of the eddy toward the north of Menorca Island in October. Eddies have a radius varying between 40 km (September 2017) and 75 km (September 2010) according to altimeter observations. While the eddy size is slightly smaller in the model than in altimetry in 2010, it is in good agreement in both datasets in 2017. In 2017 (Figure 4b) the timing and site of formation of the eddy is also consistent between model and altimetry. However, the evolution again differs between model and observations. In this case, the model shows a southeastward eddy displacement, which is not observed in the altimetry. In both datasets, the 2017 eddy is longer and more intense than the 2010 eddy, in agreement with the results from the EKE index in Figure 3.

Given the absence of data assimilation to constrain the eddy in the model (absence which is necessary here to evaluate eddy-mean flow interactions as described by the intrinsic dynamics of the model) and despite these differences between model and observations, we believe that the model representation of the eddy is sufficiently realistic in terms of eddy formation site and timing as well as lifetime during both events to provide a useful tool to further examine the generation and intensification mechanisms.

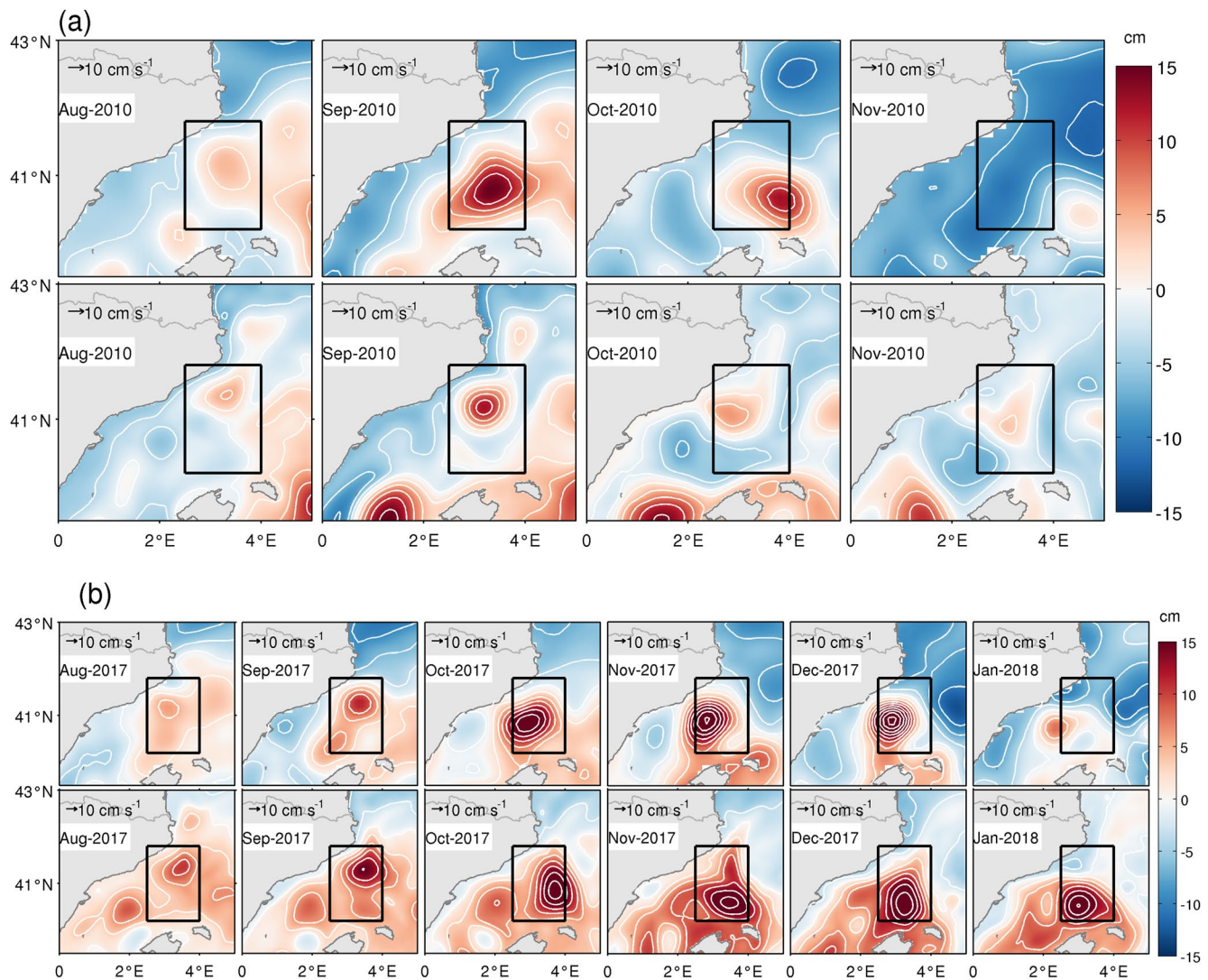


**Figure 4.** Monthly-averaged sea level anomalies (white contours depicted each 3 cm) computed from (a) August 2010 to November 2010 and, (b) from August 2017 to January 2018 using altimetry (upper row) and Western Mediterranean Operational Modeling System model data (lower row).

### 3.3. Evolution of Hydrographic Conditions

Snapshots of the SST and sea surface salinity (SSS) with SSH contours from the WMOP simulation are displayed in Figures 5 and 6 for the 2010 and 2017 events, respectively. The wind patterns obtained from the AEMET-HIRLAM model averaged during the 15 days prior to each date are also shown in these figures, together with the  $-1 \cdot 10^{-6} \text{ N/m}^3$  wind curl contour. For a more exhaustive information about the temporal and spatial evolution of these eddies the reader is referred to the SST and SSS daily animations available in the Supporting Information.

In early August 2010, a marked zonal thermal front around the  $23^\circ\text{C}$  isotherm and located around  $41.5^\circ\text{N}$  separates the colder waters to the north from the warmer waters to the south (Figure 5a). A salinity front is located farther south, bordering the northern coasts of the Balearic Islands from northeast to southwest (Figure 5b). The modeled eddy is generated in the first 2 weeks of August within the eddy-influence area, coinciding with some other small coastal anticyclonic eddies formed upstream of the Cape of Creus (Figures 5d and 5e). At the same time, a relatively warm coastal intrusion flows northward ( $41.5^\circ\text{N}$ ,  $2.5^\circ\text{E}$ ). This northward surface coastal filament just off the Cape of Begur coincides in direction with the local coastal winds that prevailed in the days prior to the formation of the eddy (Figure 5f). These winds are linked to the shadowing effect of the Pyrenees on the NW winds that blow over the Gulf of Lion, generating a weak anticyclonic atmospheric circulation between



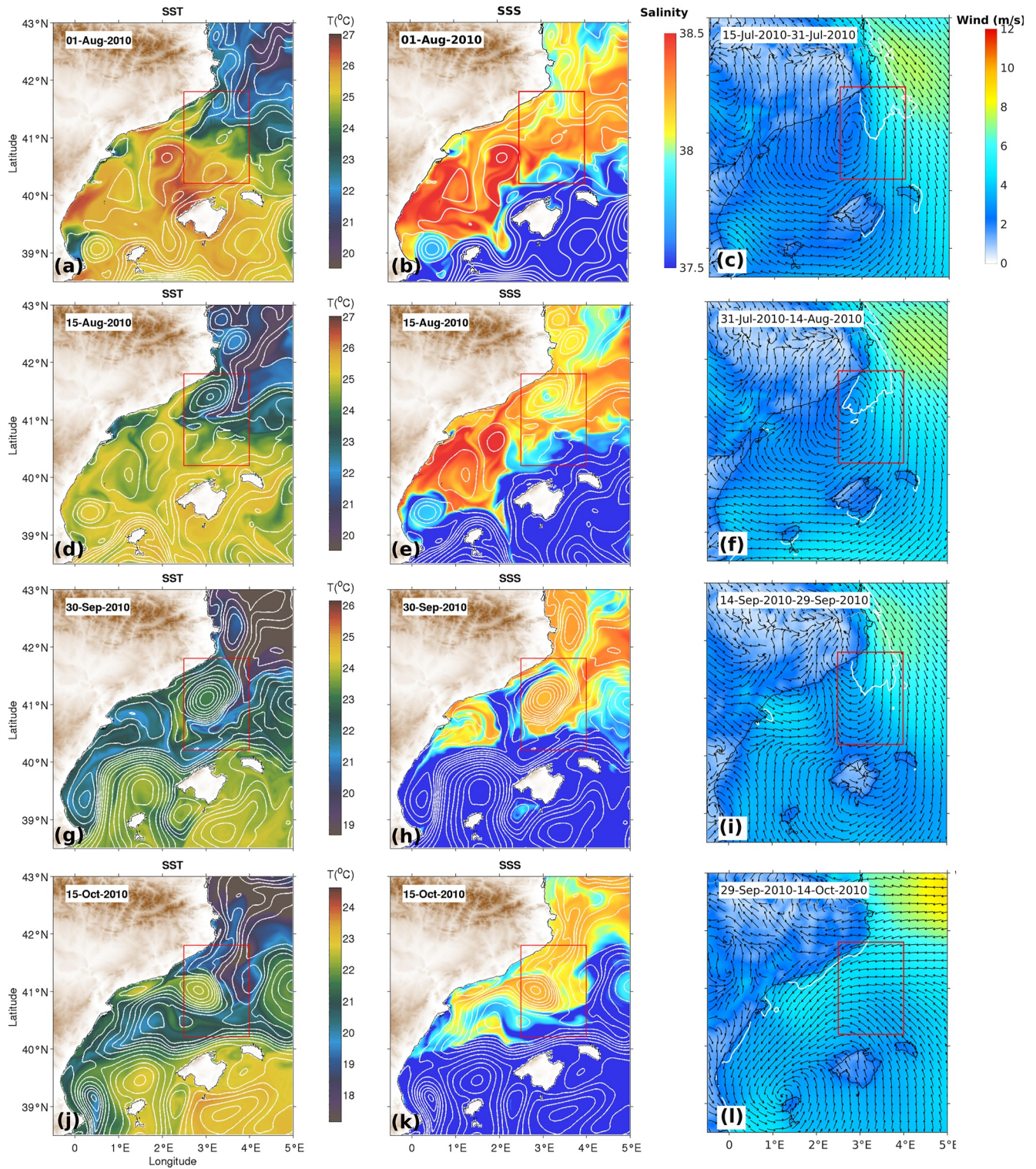


**Figure 5.** Model snapshots of [a, d, g, j] sea surface temperature and [b, e, h, k] sea surface salinity, both with sea surface height contours depicted each 2 cm (white lines), for 1 August, 15 August, 30 September and 15 October 2010 [c, f, i, l]: fortnightly averaged winds during the previous 15-day together with the  $-1 \times 10^{-6}$  wind stress curl contour in white. Red square denotes the limits of the eddy-influence area.



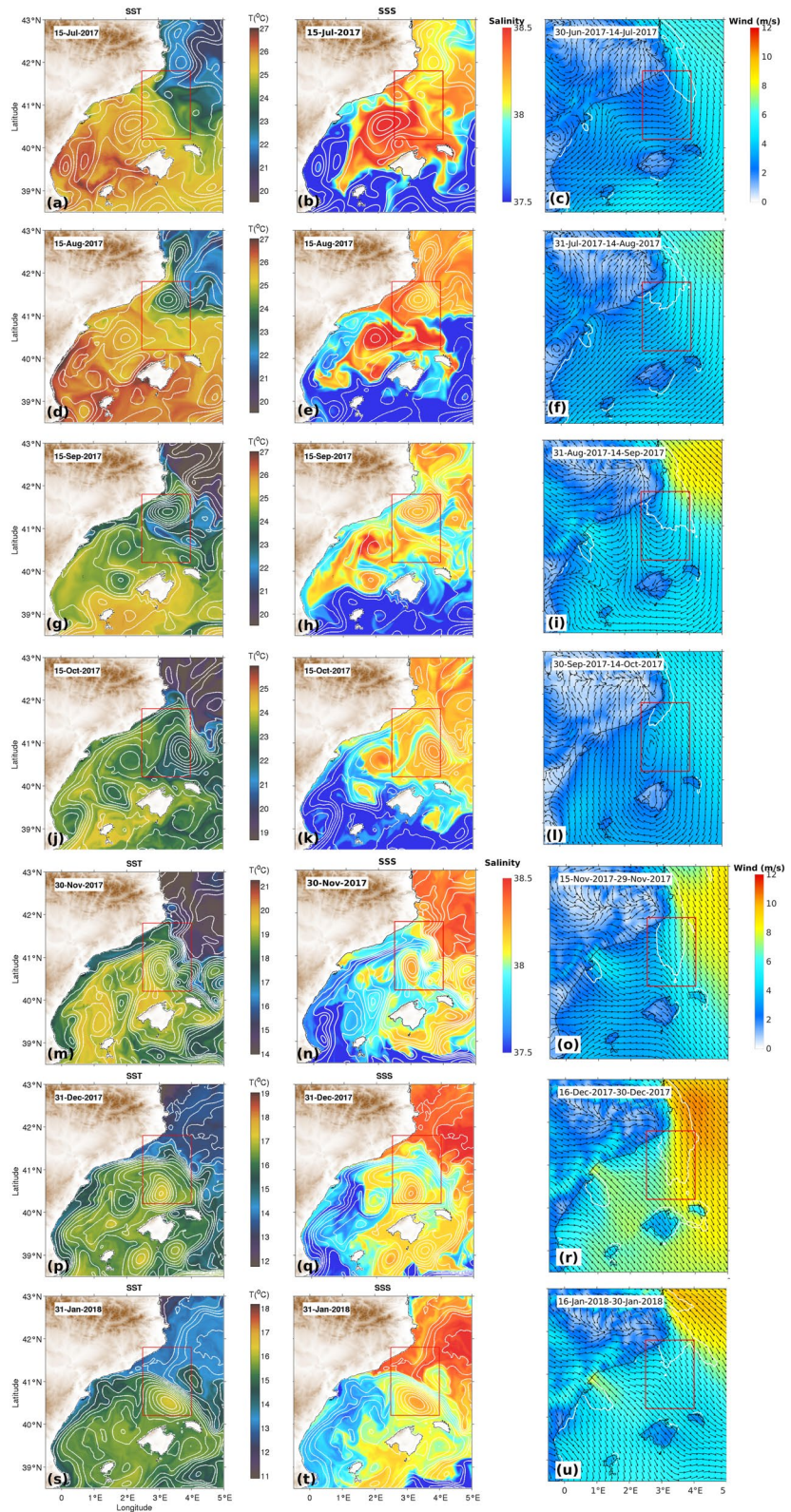


Figure 6. Same as Figure 5 for several dates along the lifetime of the 2017 eddy.

Mallorca and the Cape of Begur and an area of significant negative wind stress curl, which contributes to the generation of anticyclonic vorticity in the ocean.

The cold waters from the north enter the eddy through its south-eastern flank (Figure 5d). The salinity front remains approximately in the same area (Figure 5e). In September, the eddy grows in size and remains in the same position, the cold waters from the north continue to be entrained into the eddy (Figure 5g) and the SSS field (Figure 5h) shows northward inflows of relatively low-salinity water through the IC, probably related to the disappearance of the small eddy located north of this channel over the previous days (Figure 5e). The eddy maintains a stable position and grows in size. During this period (from mid-July to mid-September) the wind pattern is mainly characterized by (a) events of intense NW winds east of Cape of Creus, (b) a small anticyclone located between the Catalan coast and the island of Mallorca and (c) an area of significant negative wind stress curl around Cape of Begur.

The wind pattern changes at the beginning of October with northeasterly alongshore winds along the Catalan coast (Figure 5l), with a damping effect on the eddy. In November the eddy migrates southwards and finally vanishes at the end of the month (not shown).

In 2017 (Figure 6) the thermal front is established in mid-July (Figure 6a) in a similar position to that of 2010, but around the 24°C isotherm. In this case, the eddy is formed at the north of the eddy-influence area and is advected southward at the beginning of August. In mid-August (Figure 6d), a relatively warm northward coastal filament flows north at 41.5° and intensifies the anticyclonic eddy within the area. During the following month from 15 August to 15 September the eddy grows in size and remains stationary. Cold waters are entrained into the eddy on its southern side (Figure 6g), coinciding with an increase of the strength of NW winds also producing increased negative wind stress curl in the northern part of the eddy-influence area (Figure 6i).

In mid-October, the eddy moves southeastward, coinciding with an important inflow of relatively low salinity waters of recent Atlantic origin (with salinity values lower than 37.5 psu; Figure 6k). These flows do not directly enter in contact with the eddy as in 2010. While the eddy decreases in size at the end of November (Figure 6n), it grows again in December coinciding with new intense episodes of NW winds (Figure 6r).

At this moment, the thermal front has been displaced southward and is notably reinforced, showing a difference between northern and southern waters of up to 3°C. During the first days of January, the eddy remains in the same position and with the approximate same size, coinciding with weak NW winds blowing over the area (not shown). At the end of January, the strong coastal intrusion of salty and cold waters from the north displaces the eddy southeastward (Figures 6s and 6t). In February 2018 the eddy continues moving southeastward outside of the eddy-influence area before disappearing during the first days of March (shown in the animations provided in the Supporting Information).

## 4. Mechanisms and Drivers Involved in the Generation and Intensification of the Eddies

The generation and intensification mechanisms of these long-lived eddies are studied in this section by means of the analysis of (a) energy transfer terms associated with eddy-mean flow interaction, and (b) sensitivity tests aiming at relating the simulated variability of eddies with external drivers.

### 4.1. Mechanisms: Energy Transfer Terms

Figures 7 and 8 represent (a) the temporal variability and (b) the spatial patterns of the EKE and the main energy conversion terms responsible for EKE production over different periods in 2010 and 2017. These terms are referred to as: the horizontal barotropic term (T4; BT), horizontal baroclinic term (T2; BChor) and vertical baroclinic term (T3, BCvert).

In 2010 (Figure 7), the temporal evolution of the EKE shows a maximum during the last days of September, coinciding with the maximum of the BChor term (Figure 7a). This maximum is coincident with the intense Atlantic water northward inflow described in Figure 5h on 30 September 2010. The correlation coefficient of the filtered EKE and BT/BChor time series is 0.88/0.65, respectively, which also highlights the important role of BT over the whole period.



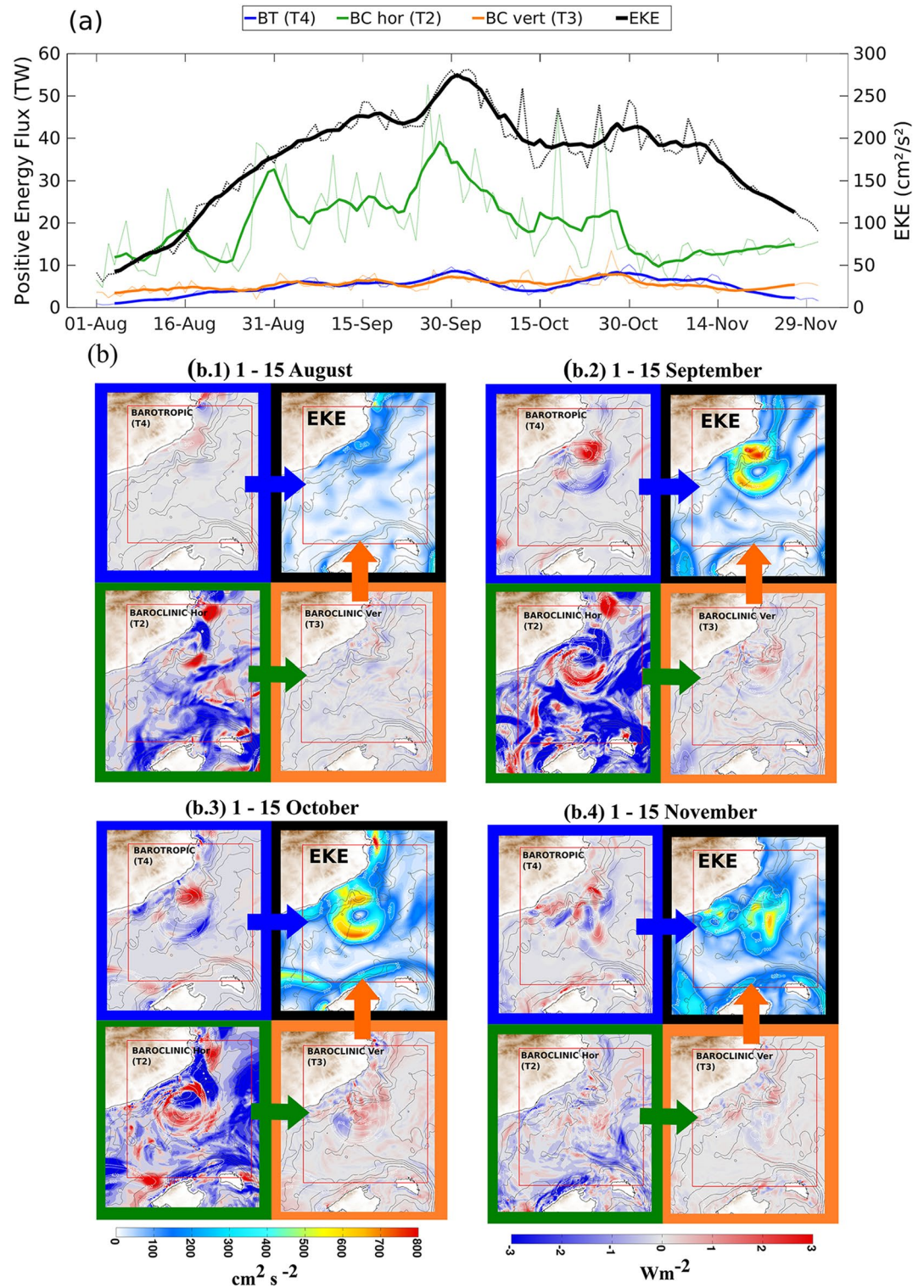


**Figure 7.** Temporal evolution (a) and spatial distribution (b) of the energy conversion terms and the eddy kinetic energy (EKE) for the year 2010. In the upper figure (a), the lines represent the positive values of each energy term (dotted line for the unfiltered signal and continuous line for the filtered signal using a 7-day moving average): in blue the barotropic term (BT; T4), in green the baroclinic horizontal term (BChor; T2), and in orange the baroclinic vertical term (BCver; T3). The black line denotes the spatially averaged EKE within the same area. The figures in panel (b) show the spatial distribution of the EKE and of each energy conversion term responsible for the EKE production at different times over the duration of the event.



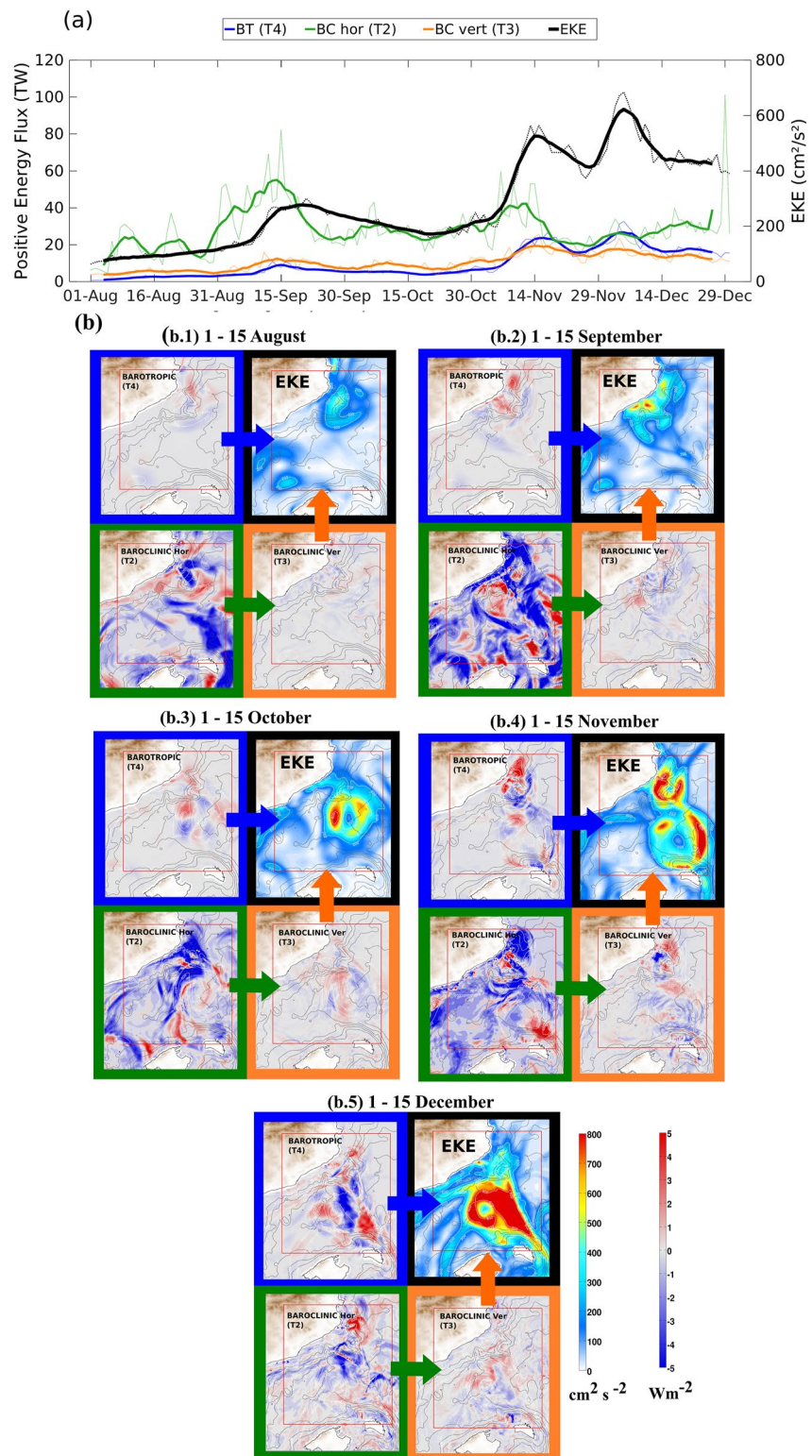


Figure 8. Same as Figure 7 for the 2017 event.

The spatial distribution of the energy terms (Figure 7b) shows that during the first days of September (Figure 7b.2), the energy of the eddy starts to increase from (a) the BT term over the shelf break in the northern part of the domain, and (b) the especially strong BChor term on the southern flank of the eddy. The EKE maintains a similar

spatial distribution until the first days of October (Figure 7b.3), although during these days the BChor term provides energy to the entire outer edge of the eddy. In November (Figure 7b.4) the eddy disappears, and both the EKE and the energy conversion terms decrease and are represented by small and scattered patches.

In 2017 (Figure 8), both the energy fluxes and EKE magnitudes are larger than during the 2010, highlighting the higher intensity of this eddy. The EKE maximum is produced during the first days of December (Figure 8a). In this case, this maximum coincides with the maximum BT term. At the beginning of the event (Figure 8b.1) the spatial patterns indicate that the energy transferred to the eddy originates mainly from the BChor term, located both to the west near the coast, and in the southern part of the eddy. The BT flux also contributes, although to a lesser extent, in the area off the Cape of Begur. The BThor term significantly increases during 1–15 September (Figure 8b.2). During 1–15 October (Figure 8b.3) the eddy moves southeastward, and the energy fluxes do not significantly change in comparison with the previous days. During the first days of November (Figure 8b.4) a new anticyclonic eddy near the coast is formed mainly through BT instability, while the previous eddy keeps growing, fed by BChor and BT fluxes. The increase of BT fluxes from mid-November, combined with the already existing BChor flux, produces an intensification of the eddy in mid-December (Figure 8b.5).

The intensification of the BT fluxes in December is coincident with the intense NW wind episodes previously described (see Figure 6o). The effect of these winds is also to mix and cool the surface layers, which in turn strengthens the thermal front (Figure 6p), also resulting in an increment of BChor in December (Figure 8a). The lifetime of this eddy is much longer than the 2010 eddy, due to increased BT and BChor terms in November and December under the action of intense NW winds, as illustrated in Figure 2. The correlation coefficient of the filtered EKE and BT/BChor time series shown in Figure 8 is 0.98/0.12, respectively, which confirms the predominant role of BT for this event compared to 2010.

Results show that the combined effect of the BT and BChor terms acting in different parts of the eddy are the main mechanisms of the generation and maintenance of these long-lived eddies. These results also highlight the importance of assessing the spatial structures of the energy conversion terms. Indeed, evaluation of the spatially averaged terms may mask the combined effect of the BT and BC instabilities.

#### 4.2. Drivers: Model Sensitivity Experiments

In the previous sections and thanks to both the temporal description of eddies and the analysis of their energy conversion terms, we related the generation and persistence of these eddies to different meteorological and oceanographic drivers, such as (a) intense NW wind events, (b) relatively warm northward coastal inflows through the Pyrenees thermal front, and (c) relatively low-salinity northward fluxes. In this section, several model sensitivity experiments were conducted in order to identify and confirm the effect of these drivers on the formation and intensification of the 2010 and 2017 eddies.

First, in order to evaluate the effect of the NW wind events, we re-ran the 2010 and 2017 simulations imposing climatological winds (configuration #1; Table 1). For a given date, these winds were computed by taking the 10-year average of the winds for this specific date over the 2009–2018 period, and by applying an additional 30-day moving-window average. These climatological winds never exceed the 12 m/s threshold in the area analyzed in Figure 2. Moreover, the average intensity of the NW component is between 40% and 60% lower than the real winds (average intensity of 3.47 m/s vs. 6.54 m/s of real winds during the 15 July–15 August period, and 3.84 m/s vs. 8.57 m/s for real winds in November). Considering the wind stress curl, values are between 81% and 93% lower in climatological winds compared to the real winds ( $-1.33 \cdot 10^{-7} \text{ N/m}^3$  vs.  $-7.06 \cdot 10^{-7} \text{ N/m}^3$  during the 15 July–15 August period, and  $-0.90 \text{ N/m}^3$  vs.  $-12.83 \cdot 10^{-7} \text{ N/m}^3$  in November 2010).

We then forced the 2010 and 2017 simulations with homogeneous temperature or salinity fields, respectively, to evaluate the impact of the thermohaline conditions on the formation and intensification of the eddy (configuration #2 and configuration #3; Table 1). The value of these constant hydrographic fields (both in surface and in depth) were defined as the spatial average over the whole simulated basin. Both the initial and boundary conditions were also affected by these changes. Moreover, in the case of constant temperature, the atmospheric heat fluxes were also defined as spatially homogeneous over the basin to avoid the formation of thermal fronts. Finally, a last configuration imposed both homogeneous salinity and climatological winds for 2017 during the intensification phase in order to evaluate the effects of the NW winds events on the intensification of the 2017

**Table 1**

*Results of the Sensitivity Experiments Carried Out From July–December 2010 and 2017 to Evaluate the Effect of the Main Forcings on the Eddy Generation and Intensification*

|             | Winds          | Temp.       | Salt        | Eddy identification |        |           |                 |                 |
|-------------|----------------|-------------|-------------|---------------------|--------|-----------|-----------------|-----------------|
|             |                |             |             | July                | August | September | Oct             | Nov             |
| <b>2010</b> | Reference      | Reference   | Reference   | x                   | ✓      | ✓✓        | ✓✓              | ✓               |
| <b>#1</b>   | Climatological | Reference   | Reference   | x                   | x      | X         | X               | X               |
| <b>#2</b>   | Reference      | Homogeneous | Reference   | x                   | ✓      | X         | X               | X               |
| <b>#3</b>   | Reference      | Reference   | Homogeneous | x                   | ✓      | ✓✓        | X               | ✓✓ <sup>a</sup> |
| <b>2017</b> | Reference      | Reference   | Reference   | x                   | ✓✓     | ✓✓✓       | ✓✓✓             | ✓✓✓             |
| <b>#1</b>   | Climatological | Reference   | Reference   | x                   | X      | X         | X               | X               |
| <b>#2</b>   | Reference      | Homogeneous | Reference   | x                   | X      | X         | ✓✓ <sup>a</sup> | X               |
| <b>#3</b>   | Reference      | Reference   | Homogeneous | x                   | ✓✓     | ✓✓✓       | ✓✓✓             | ✓✓✓             |
| <b>#4</b>   | Climatological | Reference   | Homogeneous |                     |        | ✓✓        | ✓✓              | ✓✓              |

*Note.* Cross indicates the absence of eddy while single/double/triple tick indicates a low/moderate/high intensity eddy, based on its surface spatially averaged SLA signature (✓:  $SLA \leq 4$  cm, ✓✓:  $4 < SLA \leq 10$  cm, ✓✓✓:  $SLA > 10$  cm).

<sup>a</sup>Indicates cases in which the OW method detects eddies that have a different origin from the eddy of interest.

eddy. Configurations #1 to #3 were initialized on 1 July (2010 or 2017), before the eddy formation, from the fields of the reference simulation, and ended at the end of November to represent both the eddy generation and intensification periods. Configuration #4 was initialized from the reference fields on 1 September 2017 after the eddy was formed to specifically focus on the intensification period.

In order to evaluate the presence or absence of the eddy in the different tests, we applied the Okubo-Weiss detection method (see Section 2.5). Once the eddy is detected, the OW contours define the eddy signature and the maximum value of SLA marks the eddy center. The spatially averaged SLA within the signature of the eddy provides the intensity of the eddy. Only values within a radius of  $0.2^\circ$  from the eddy center are considered to avoid interferences with small adjacent eddies. The results of these experiments are illustrated in Appendix A and summarized in Table 1.

No eddy is formed in Configuration #1 using climatological winds, neither in 2010 nor in 2017 (see maps in Appendix A1). This result confirms that the NW wind events are one of the necessary contributors for the eddy formation in this area. In Configuration #2, no eddy is formed when the thermal gradients are artificially removed in both simulations (see maps in Appendix A2), which also confirms the necessity of a thermal front in order to generate the eddy in both years. It is also worth mentioning that the eddy that was located south-west of the eddy influence area in October 2017 persists despite the absence of temperature gradients and moves northeastward, entering the eddy influence area (see \* in Table 1).

Configuration #3 generates an eddy in both 2010 and 2017 cases, indicating that salinity gradients are not necessary for the generation of these eddies (Appendix A3). However, there are substantial differences between both years: in 2010, the simulation with constant salinity does not lead to eddy intensification as in the reference simulation, demonstrating that salinity gradients played a crucial role in the intensification of the eddy. On the contrary, in 2017 the eddy is generated and strengthened even in the absence of salinity gradients. The eddy intensification in 2017 is therefore related to winds and/or temperature gradients.

Configuration #4 imposing climatological winds and homogeneous salinity fields from 1 September (after the eddy formation) tells us about the impact of NW wind episodes on the intensification of the 2017 eddy. Climatological winds only lead to a moderate strength eddy (see maps in Appendix A4), demonstrating that the NW winds events had an important role in the intensification of the eddy during this year.

Table 2 shows the values of the average vertical shear of the horizontal velocities in the upper 100m of the eddy-influence area for the period 15 July–15 August in the different simulations in 2010 and 2017. This vertical shear, which provides favorable conditions for the development of baroclinic instabilities, is significantly

**Table 2**

Vertical Shear of the Horizontal Velocities, Computed as  $\sqrt{\left(\frac{\partial u}{\partial z}\right)^2 + \left(\frac{\partial v}{\partial z}\right)^2}$ , Averaged Over the Upper 100m in the Eddy Influence Area for the Period 15 July to 15 August in 2010 and 2017 for the Different Simulations

| Year | Reference | Configuration #1 | Configuration #2 | Configuration #3 |
|------|-----------|------------------|------------------|------------------|
| 2010 | 2.5       | 1.1              | 1.4              | 2.3              |
| 2017 | 2.2       | 1.0              | 1.3              | 2.3              |

Note. The unit is  $10^{-3} \text{ s}^{-1}$ .

reduced when imposing climatological winds and homogeneous temperatures, explaining why the eddies do not form in configurations #1 and #2. The effect is smaller when imposing homogeneous salinity fields.

In summary, these sensitivity model simulations help identify the drivers implicated in each event, providing support to the previous results. They demonstrate that the NW wind events and the existence of a thermal front were both necessary conditions for the formation of the eddy in this area in 2010 and 2017. The 2010 and 2017 eddies featured two different situations concerning their intensification: while in 2010 salinity gradients were necessary to intensify and maintain the eddy, they had no significant role in 2017. The final experiment showed that in 2017 the NW winds were an important driver responsible for the eddy intensification.

## 5. Discussion

In this study we have investigated the coupled eddy-mean flow system that typically forms south of Cape of Begur at the end of summer. The temporal evolution of the eddies and the study of their energy conversion terms allow us to relate the generation and persistence of the 2010 and 2017 eddies with NW winds, warm water inflows, and low-salinity northward fluxes. These drivers were then further identified by evaluating different configurations of the high-resolution WMOP numerical model.

Scenario for the development and intensification of strong long-lived anticyclonic eddies.

Our results show that both NW wind events and thermal gradients are necessary for the generation of these eddies but that the intensification process was different for 2010 and 2017. The eddy-mean flow interactions in Figures 7 and 8 show that, in 2010, the energy needed for the eddy intensification came mainly from the BC term, while in 2017 the BT term was also an important source of energy during the intensification of the eddy (from mid-November). The evaluation of the spatial distribution of the energy conversion terms (Figures 7b and 8b) combined with the spatial and temporal description of the hydrographic and wind maps (Figures 5 and 6) is helpful to interpret how these eddy generation mechanisms act in the study area. BT instability, occurring mainly near the coast, is associated with horizontal gradients of the flow that produce a transfer of kinetic energy from the mean flow to the eddy. In this area, these flow variations are related to deviations of the NC off the Cape of Begur (Aguiar et al., 2019) under the action of intense NW winds. On the other hand, the eddy also gains energy from the mean flow through BC instability produced by the warm northward inflows that reach the Pyrenees thermal front and/or by relatively low-salinity waters that come from the south.

The model sensitivity tests confirm these hypotheses demonstrating that the presence of the NW winds is a necessary condition for eddy generation, but it is not sufficient. The presence of the Pyrenees thermal front is also necessary to create the required baroclinic gradients for the generation of these eddies. This explains the observed seasonality of the eddy generation, the thermal front being particularly intense at the end of the summer due to the large summer differential warming and mixing between the BS and the Gulf of Lion (López-García et al., 1994). Once the eddy is formed, it imports energy from different sources. In 2010, this extra energy came from BC instability produced by the arrival of low-salinity waters coming from the south, which are favored by the presence of the eddy (since its presence helps to steer the NC eastward). In 2017, the intensification of the eddy was a result of additional intense NW wind events in November. These winds exerted both mechanical surface forcing that accelerated and cooled the eddy, leading to a strengthening of the thermal front between the Gulf of Lion and the BS. These scenarios are depicted schematically in Figure 9.

Our results endorse the hypothesis previously proposed by Pascual et al. (2002) from an analysis of satellite images and hydrographic data. They investigated the 1998 long-lived eddy and suggested that the NW winds combined with the presence of waters of recent Atlantic origin close to the Pyrenees were the main factors for the eddy generation. Our results extend the results of Rubio et al. (2009), who described the generation mechanisms of a short-lived eddy generated off Cape of Creus in a simulation of the summer 2002, as a combination of barotropic and horizontal baroclinic instabilities. While they identified the winds as an essential driver needed to generate the eddy, they suggested that the eddy growth could be associated with baroclinic instability. Our results



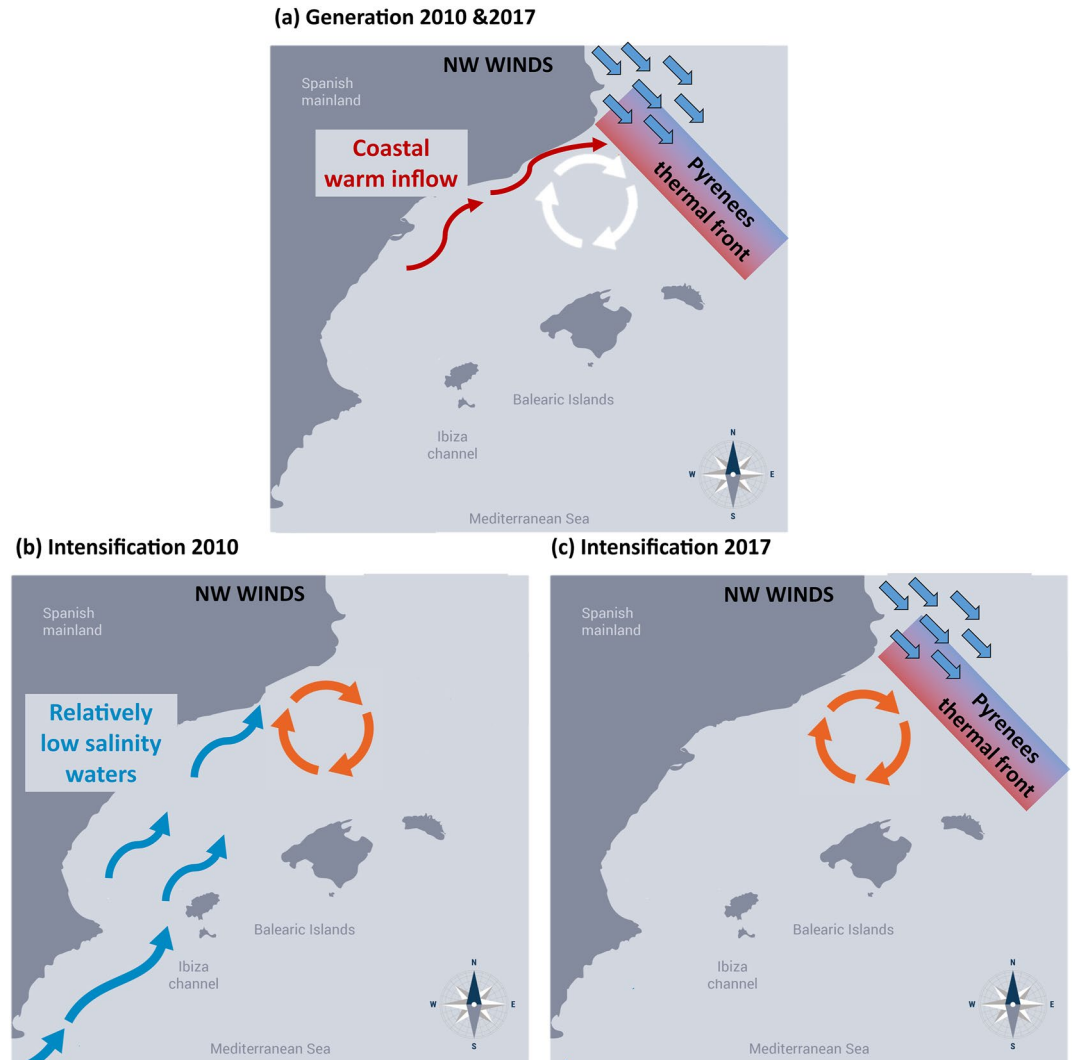


**Figure 9.** Proposed scenario for the development and intensification of long-lived anticyclonic eddies at the end of the summer in the Balearic Sea (BS). The generation of eddies is a result of (1) barotropic instability of the Northern Current under the effect of intense Northwesterly (NW) winds, and (2) baroclinic instability associated with the relatively warmer northward inflows that reach the Pyrenees thermal front. The intensity and duration of the two eddies differed between the two years: in 2010 these properties were driven by the inflows of low-salinity waters from the south which fed the eddy; in 2017, additional energy was provided by the intense NW winds events, which kept the eddy active and reinforced the thermal front between the Gulf of Lions and the BS.

are also consistent and provide an extension of Garreau et al. (2011), who investigated an eddy formed in the southwestern part of the Gulf of Lion and propagating southwards into the BS in autumn 2007, explaining the generation as a combination of NW winds over this area with accumulation of potential energy, also identifying the role of a relatively warm northward coastal current in the formation process. Here, focusing on two identified strong and long-lived events, we further demonstrate the role of winds, thermal gradients, and low salinity inflows on both the formation and intensification of the BS eddies, highlighting significant differences between the two events. Notice that in the Eastern Mediterranean Sea, Ioannou et al. (2020a, 2020b) also reported intense and recurrent mesoscale anticyclones in the lee of Crete forced by an orographic wind jet produced by the channeling and deflection of the Etesian winds by the island, showing similarities with the orographic effect of the Pyrenees as highlighted here. The authors confirmed that these winds were necessary but not sufficient to form the eddies and suggested that this mechanism had to be reinforced by some other baroclinic process.

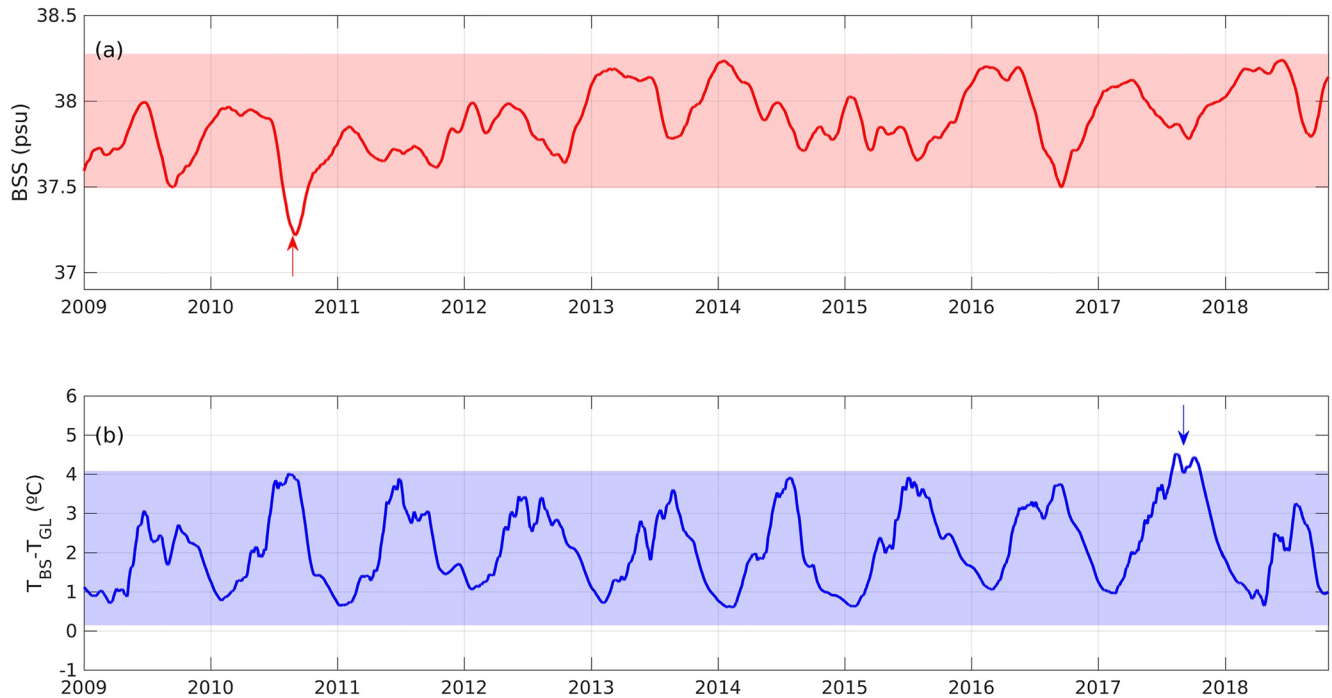


**Figure 10.** Interannual time-series from the Western Mediterranean Operational Modeling System model of (a) spatially averaged surface salinity within the Balearic Sea (BS), and (b) the difference between the average temperature in the BS and the Gulf of Lion. The shaded areas mark the mean  $\pm$  two standard deviations of the time-series. Values outside this area are considered to be anomalous. The time-series are temporally filtered using a 30-day moving average.

### 5.1. Specific Hydrographic and Meteorological Conditions for the Development of Strong Long-Lived Eddies

The specificities of the hydrographic conditions in 2010 and 2017 are illustrated in Figure 10.

On the one hand, in October 2010, the intrusion of the low-salinity waters from the south is identified as an anomalous event (red arrow in Figure 10a, minimum 37.2 psu on 2 October), which is not reproduced at any time of the 10-year time-series. On the other hand, the reinforced Pyrenees thermal gradients are also identified as anomalously high in 2017.

The low-salinity waters detected in the BS in 2010 came from the Atlantic through the Gibraltar strait and then through the Ibiza and Mallorca channels (Barceló-Llull et al., 2019; Heslop et al., 2012; Juza et al., 2019; Mason & Pascual, 2013). The presence of the eddy could reinforce this inflow of low-salinity waters since the NC deviates from its natural path, modifying the circulation in the BS and favoring the entrance of Atlantic Water (Aguiar et al., 2019). At this point, it is worth pointing out the reported presence of the Portuguese Man-of-War (*Physalia Physalia*) in the Western Mediterranean Sea in 2010. This species is not common within the BS but, according to Prieto et al. (2015), it entered the basin in 2010 due to intense westerly winds blowing in the Strait of Gibraltar, which were 1.5–4 times higher than the long-term average. The authors related these intense winds to the anomalously negative values of the North Atlantic Oscillation (NAO) index during the 2010 winter. We can expect these winds to also increase the inflow transport through the Strait of Gibraltar, which would in turn lead to larger amounts of relatively low-salinity waters in the BS, contributing to strengthen the EKE through baroclinic instabilities. This relation between climatological indices and the modulation of the oceanic variability has been also reported in other areas (Chen et al., 2020; Peng et al., 2019). In our case, a preliminary analysis of the NAO index during both events shows that it was mainly negative for both years, although slightly less intense during 2017 ( $NAO_{Aug-Nov2010} = -1.16$ ,  $NAO_{Aug-Nov2017} = -0.35$ ). A more detailed analysis would be needed to establish possible links between the NAO index and the presence of these long-lived eddies.

In 2017, while inflows of low-salinity waters were detected through the IC, they did not directly interact with the eddy as they did in 2010. In this case, the intensification process was driven by the extra intense NW winds blowing in November 2017, which were stronger compared to 2010 (Figure 2). The impact of these additional

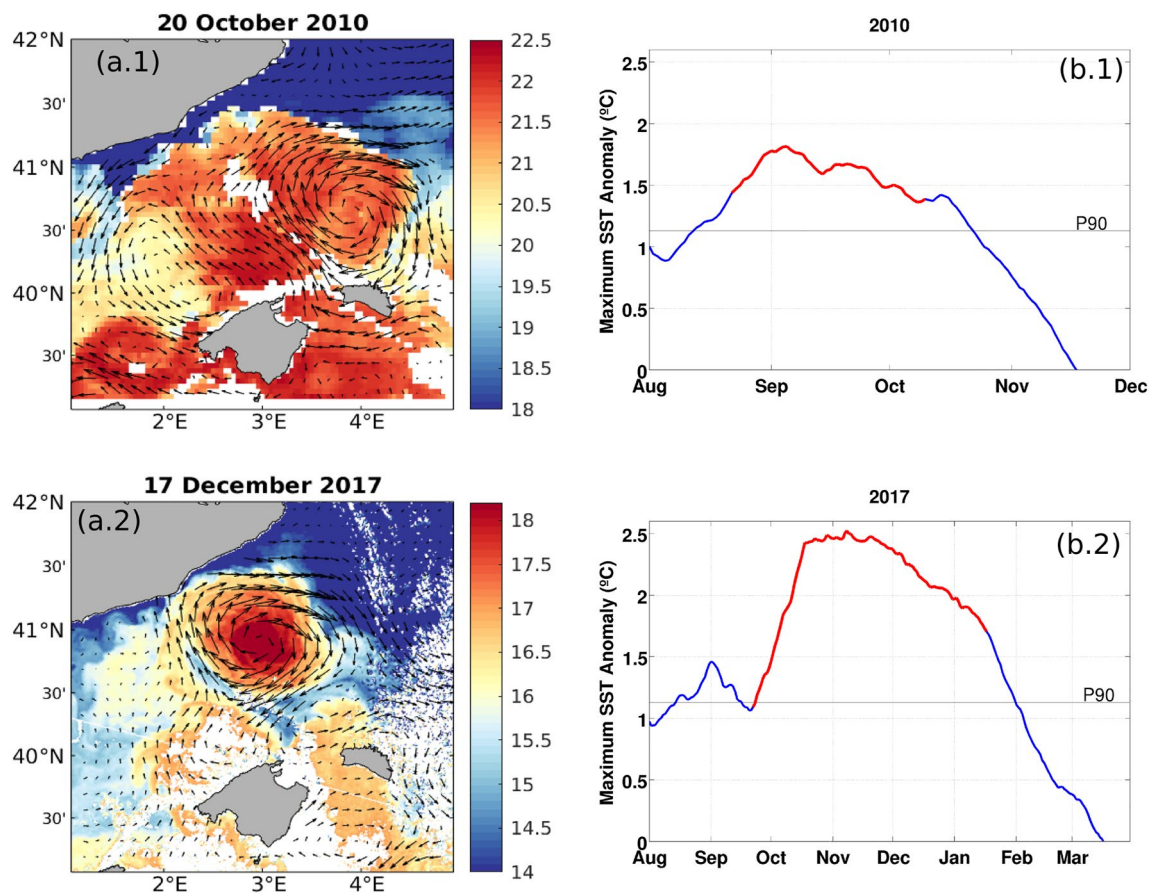


**Figure 11.** (a) Sea surface temperature (SST) ( $^{\circ}\text{C}$ ) from satellite data on 20 October 2010 (a.1) and on 17 December of 2017 (a.2), (b) Maximum SST anomalies within the eddy-influence area during the 2010 (b.1) and the 2017 (b.2) events. Anomalies are computed with respect to the average seasonal cycle over the period 2009–2018 and are detrended and low-pass filtered using a 30-day moving average. The red lines indicate the presence of the eddies as detected by altimetry according to the criterion defined in Section 3.1. The horizontal lines denote the 90th percentile of the 2009–2018 anomalies ( $1.13^{\circ}\text{C}$ ).

intense NW winds is also reflected in the evolution of the BT term in Figures 7 and 8, with a significant increase in November in 2017, which does not happen in 2010.

### 5.2. Thermal Impacts of Intense Long-Lived Eddies

The eddies studied in this work have a potential impact on coastal ecosystems given their capacity to trap water masses, modify hydrodynamics and alter coastal cross-shelf exchange. The water trapped inside an eddy during its formation is preserved within the eddy as it propagates away from its generation location. Temperature and salinity anomalies inside individual eddies tend to move with them because of advective trapping of interior water parcels, the eddy movements then driving heat and salt transports (Dong et al., 2014). Here, the SST obtained from satellite data on 20 October 2010 and on 17 December 2017 (Figure 11a.1 and 11a.2) demonstrates that during these events, the eddies have strong thermal signatures, with differences of about  $3^{\circ}\text{C}$  between the core and the outer part of the eddy. Differences of this magnitude were also detected in the model simulation (Figures 5j, 15 October 2010 and Figures 6p, 31 December 2017). Time series of the maximum SST anomaly in the eddy-influence area with respect to the average seasonal cycle (Figure 11b.1 and 11b.2) also demonstrate the significant thermal signatures of these eddies. Notice that these time series were previously detrended to remove the impact of the positive and significant trend associated with Mediterranean climate warming. High SST anomalies coincide with the presence of the eddies as detected by altimetry (red lines in the time series) during both years. While maximum values of the anomalies are about  $1.8^{\circ}\text{C}$  in 2010, they reach almost  $2.5^{\circ}\text{C}$  during more than one month in 2017. Comparisons with the 90th percentile of 2009–2018 anomalies ( $1.13^{\circ}\text{C}$ ) show that this threshold is exceeded during both years during the eddy lifetimes. The 90th percentile is a reference

value generally used to define marine heatwaves (Hobday et al., 2016). Although the time series considered here is limited compared to the more than 30 years-long time series used to rigorously define heatwaves, our results suggest that the presence of these eddies contributed significantly to the occurrence of local heatwaves during the autumn of 2010 and winter of 2017–2018.

The impacts of the thermal environment and heatwaves on marine biota is an active research field in the Mediterranean Sea. Bensoussan et al. (2019b) reported an unprecedented large-scale and long-lasting benthic mucilaginous bloom that occurred in the north Catalan Sea during fall 2017. They associated this event with an anomalously high temperature in the area, which was suggested to be related to the presence of the long-lived eddy described in this study. Other studies also associated small temperature anomalies in the Mediterranean Sea with dramatic mass mortality in benthic ecosystems (Parravicini et al., 2010), in subtidal rocky reef invertebrates (Cerrano et al., 2000; Garrabou et al., 2009; Pérez et al., 2000) or in seagrass shoots (Marbà & Duarte, 2010). Among other effects and although there is no established evidence yet, these surface warm water parcels may also influence the weather and storm development in this area given demonstrated air-sea interactions over ocean fronts and eddies (e.g., Small et al., 2008 and references therein). The impact of these eddies on the retention of materials and alteration of coastal cross-shelf transports would certainly also be an interesting topic of research in the future.

## 6. Summary and Conclusions

Numerical models are valuable tools to analyze the details of the generation and growth of intense long-lived eddies. They provide a full description of eddy evolution that allows us to evaluate eddy-mean flow interactions, conduct sensitivity tests, and to relate the simulated variability to external forcings. In this study, they have been used to demonstrate that the two most recent strong and long-lived anticyclonic eddies occurring in 2010 and 2017 in the BS were a result of mixed barotropic and baroclinic instabilities. Specifically, we have identified the drivers that explain the development and intensification of these two strong long-lived anticyclonic eddies. Our results indicate that the required conditions for eddy generation in this area were the same for both events: intense NW winds blowing over an area characterized by an intense thermal front formed during the summer season. However, regarding eddy intensification, different mechanisms were active for each eddy. In 2010 the presence of relatively low-salinity waters in the BS was the main factor intensifying the eddy. In 2017, the strength and persistence of the eddy was associated with additional intense NW winds events which occurred until December, and which both exerted mechanical surface forcing and strengthened the thermal front between the Gulf of Lions and the BS. The presence of the eddies in 2010 and 2017 resulted in long-lasting surface thermal anomalies above the 90th percentile of the time series, corresponding to the definition of local marine heatwaves, with maximum values of the anomalies around 2.5°C during the winter 2017.

## Appendix A: Model Sensitivity Experiments

Results of the sensitivity experiments carried out from July to December of 2010 and 2017 to evaluate the effect of the main forcings on eddy generation and intensification. The maps show the monthly -averaged SLA (white contours depicted each 2 cm). Blue contours indicate the signature of the eddy by means of OW values lower than the threshold (OW<sub>0</sub>) and within a radius of 0.2° from the eddy center. Black square denotes the area of eddy generation reported in Figure 1.

### A1. Reference Years

Monthly-averaged SLA maps for the reference simulations.

### A2. Configuration #1

Monthly-averaged SLA maps for the simulations forced using climatological winds.

### A3. Configuration #2

Monthly-averaged SLA maps for the simulations forced using homogeneous temperature.



#### A4. Configuration #3

Monthly-averaged SLA maps for the simulations forced using homogeneous salinity.

#### A5. Configuration #4

Monthly-averaged SLA maps for the simulations forced using climatological winds and homogeneous salinity.

### Data Availability Statement

The Western Mediterranean Operational Modelling System model simulation and sensitivity tests are stored in SOCIB repositories and available upon request.

#### Acknowledgments

This work was supported by the La Caixa foundation through the MEDCLIC project (LCF/PR/PR14/110900). A. Pascual acknowledges support from the Spanish Research Agency and the European Regional Development Fund (Award no. CTM2016-78607-P). The authors thank AEMET, the Spanish Meteorological Agency, for providing the HIRLAM wind fields and CMEMS for satellite altimetry and satellite sea surface temperature products (<https://marine.copernicus.eu/>). The authors thank Adèle Révelard, Alex Santana, Máximo García-Jove, Mélanie Juza and Jaime Hernández Lasheras for useful discussions and technical support. We also thank the anonymous reviewers whose valuable suggestions and comments helped improve and clarify this manuscript.

### References

- Aguilar, E., Juza, M., Mourre, B., Pascual, A., Mason, E., Alvera-Azcárate, A., & Tintore, J. (2019). Anticyclonic eddy anomaly: Impact on the boundary current and circulation in the Western Mediterranean Sea. In The Copernicus marine environment Monitoring Service ocean state report, Issue3. *Journal of Operational Oceanography*, 12(sup1), S1–S123. <https://doi.org/10.1080/1755876X.2019.1633075>
- Aguilar, E., Mourre, B., Juza, M., Reyes, E., Hernández-Lasheras, J., Cutolo, E., et al. (2020). Multi-platform model assessment in the Western Mediterranean Sea: Impact of downscaling on the surface circulation and mesoscale activity. *Ocean Dynamics*. <https://doi.org/10.1007/s10236-019-01317-8>
- Amitai, Y., Lehahn, Y., Lazar, A., & Heifetz, E. (2010). Surface circulation of the eastern Mediterranean Levantine basin: Insights from analyzing 14 years of satellite altimetry data. *Journal of Geophysical Research*, 115, C10058. <https://doi.org/10.1029/2010JC006147>
- Ballarotta, M., Ubelmann, C., Pujol, M.-I., Taburet, G., Fournier, F., Legeais, J.-F., et al. (2019). On the resolutions of ocean altimetry maps. *Ocean Science*, 15(4), 1091–1109. <https://doi.org/10.5194/os-15-1091-2019>
- Barceló-Llull, B., Pascual, A., Ruiz, S., Escudier, R., Torner, M., & Tintoré, J. (2019). Temporal and spatial hydrodynamic variability in the Mallorca channel (Western Mediterranean Sea) from 8 Years of underwater glider data. *Journal of Geophysical Research: Oceans*, 124(4), 2769–2786. <https://doi.org/10.1029/2018JC014636>
- Beckmann, A., Böning, C. W., Brügge, B., & Stammer, D. (1994). On the generation and role of eddy variability in the central North Atlantic Ocean. *Journal of Geophysical Research*, 99(C10), 20381–20391. <https://doi.org/10.1029/94JC01654>
- Bensoussan, N., Chiggiato, J., Buongiorno Nardelli, B., Pisano, A., & Garrabou, J. (2019). Insights on 2017 marine heat waves in the Mediterranean Sea. Copernicus Marine Service Ocean State Report #3. *Journal of Operational Oceanography*.
- Brach, L., Deixonne, P., Bernard, M.-F., Durand, E., Desjean, M.-C., Perez, E., et al. (2018). Anticyclonic eddies increase accumulation of microplastic in the North Atlantic subtropical gyre. *Marine Pollution Bulletin*, 126, 191–196. <https://doi.org/10.1016/j.marpolbul.2017.10.077>
- Buongiorno Nardelli, B., Tronconi, C., Pisano, A., & Santoleri, R. (2013). High and ultra-high resolution processing of satellite sea surface temperature data over southern European seas in the framework of MyOcean project. *Remote Sensing of Environment*, 129, 1–16. <https://doi.org/10.1016/j.rse.2012.10.012>
- Capet, A., Mason, E., Rossi, V., Troupin, C., Faugère, Y., Pujol, I., & Pascual, A. (2014). Implications of refined altimetry on estimates of mesoscale activity and eddy-driven offshore transport in the Eastern Boundary Upwelling Systems. *Geophysical Research Letters*, 41(21), 7602–7610. <https://doi.org/10.1002/2014GL061770>
- Capó, E., Orfila, A., Mason, E., & Ruiz, S. (2018). Energy conversion routes in the Western Mediterranean Sea estimated from eddy–mean flow interactions. *Journal of Physical Oceanography*, 49(1), 247–267. <https://doi.org/10.1175/JPO-D-18-0036.1>
- Cerrano, C., Bavestrello, G., Bianchi, C. N., Cattaneo-vietti, R., Bava, S., Morganti, C., et al. (2000). A catastrophic mass-mortality episode of Gorgonian and other organisms in the Ligurian Sea (North-western Mediterranean), summer 1999. *Ecology Letters*, 3(4), 284–293. <https://doi.org/10.1046/j.1461-0248.2000.00152.x>
- Chelton, D. B., DeSzoeko, R. A., Schlax, M. G., El Naggar, K., & Siwertz, N. (1998). Geographical variability of the first baroclinic Rossby radius of deformation. *Journal of Physical Oceanography*, 28(3), 433–460. [https://doi.org/10.1175/1520-0485\(1998\)028<0433:gvotfb>2.0.co;2](https://doi.org/10.1175/1520-0485(1998)028<0433:gvotfb>2.0.co;2)
- Chelton, D. B., Gaube, P., Schlax, M. G., Early, J. J., & Samelson, R. M. (2011). The influence of nonlinear mesoscale eddies on near-surface oceanic chlorophyll. *Science*, 334(6054), 328. <https://doi.org/10.1126/science.1208897>
- Chelton, D. B., Schlax, M. G., & Samelson, R. M. (2011). Global observations of nonlinear mesoscale eddies. *Progress in Oceanography*, 59(2), 167–216. <https://doi.org/10.1016/j.pocean.2011.01.002>
- Chen, G., Wang, D., Han, W., Feng, M., Wang, F., Li, Y., & Gordon, A. L. (2020). The extreme El Niño events suppressing the intraseasonal variability in the eastern tropical Indian Ocean. *Journal of Physical Oceanography*, 50(8), 2359–2372. <https://doi.org/10.1175/jpo-d-20-0041.1>
- Condie, S., & Condie, R. (2016). Retention of plankton within ocean eddies. *Global Ecology and Biogeography*, 25(10), 1264–1277. <https://doi.org/10.1111/geb.12485>
- Dong, C., McWilliams, J. C., Liu, Y., & Chen, D. (2014). Global heat and salt transports by eddy movement. *Nature Communications*, 5(1), 3294. <https://doi.org/10.1038/ncomms4294>
- d’Ovidio, F., Monte, S. D., Penna, A. D., Cotté, C., & Guinet, C. (2013). Ecological implications of eddy retention in the open ocean: A Lagrangian approach. *Journal of Physics A: Mathematical and Theoretical*, 46(25), 254023. <https://doi.org/10.1088/1751-8113/46/25/254023>
- Escudier, R., Renault, L., Pascual, A., Brasseur, P., Chelton, D., & Beuvier, J. (2016). Eddy properties in the Western Mediterranean Sea from satellite altimetry and a numerical simulation. *Journal of Geophysical Research: Oceans*, 121(6), 3990–4006. <https://doi.org/10.1002/2015JC011371>
- Ferrari, R., & Wunsch, C. (2009). Ocean circulation kinetic energy: Reservoirs, sources, and sinks. *Annual Review of Fluid Mechanics*, 41(1), 253–282. <https://doi.org/10.1146/annurev.fluid.40.111406.102139>
- Font, J., Salat, J., & Tintoré, J. (1988). Permanent features of the circulation in the Catalan Sea. *Oceanologica Acta, Special issue*.

- Fox-Kemper, B., Palter, J. B., Marsland, S., Chassignet, E., Curchitser, E., Griffies, S., & Weijer, W. (2019). In J. Zhu, M. Patterson, & L. Ying (Eds.), *Sources and sinks of ocean mesoscale eddy energy: A joint US CLIVAR and CLIVAR workshop report (No. 2019-5)*. U.S. CLIVAR Project Office. <https://doi.org/10.5065/ch5r-5034>
- Garrabou, J., Coma, R., Bensoussan, N., Bally, M., Chevaldonné, P., Cigliano, M., et al. (2009). Mass mortality in Northwestern Mediterranean rocky benthic communities: Effects of the 2003 heat wave. *Global Change Biology*, 15(5), 1090–1103. <https://doi.org/10.1111/j.1365-2486.2008.01823.x>
- Garreau, P., Garnier, V., & Schaeffer, A. (2011). Eddy resolving modelling of the Gulf of Lions and Catalan sea. *Ocean Dynamics*, 61(7), 991–1003. <https://doi.org/10.1007/s10236-011-0399-2>
- Gaube, P., Barcelo, C., McGillicuddy, D. J., Jr., Domingo, A., Miller, P., Giffoni, B., et al. (2017). The use of mesoscale eddies by juvenile loggerhead sea turtles (*Caretta caretta*) in the southwestern Atlantic. *PLoS One*, 12(3). <https://doi.org/10.1371/journal.pone.0172839>
- Gaube, P., Braun, C. D., Lawson, G. L., McGillicuddy, D. J., Penna, A. D., Skomal, G. B., et al. (2018). Mesoscale eddies influence the movements of mature female white sharks in the Gulf Stream and Sargasso Sea. *Scientific Reports*, 8(1), 7363. <https://doi.org/10.1038/s41598-018-25565-8>
- Gaube, P., & McGillicuddy, D. J. (2017). The influence of Gulf Stream eddies and meanders on near-surface chlorophyll. *Deep Sea Research Part I: Oceanographic Research Papers*, 122, 1–16. <https://doi.org/10.1016/j.dsr.2017.02.006>
- Gaube, P., McGillicuddy, D. J., Jr., Chelton, D. B., Behrenfeld, M. J., & Strutton, P. G. (2014). Regional variations in the influence of mesoscale eddies on near-surface chlorophyll. *Journal of Geophysical Research: Oceans*, 119(12), 8195–8220. <https://doi.org/10.1002/2014jc010111>
- Greatbatch, R. J. (1987). A model for the inertial recirculation of a gyre. *Journal of Marine Research*, 45(3), 601–634. <https://doi.org/10.1357/002224087788326821>
- Heslop, E. E., Ruiz, S., Allen, J., López-Jurado, J. L., Renault, L., & Tintoré, J. (2012). Autonomous underwater gliders monitoring variability at “choke points” in our ocean system: A case study in the western Mediterranean Sea. *Geophysical Research Letters*, 39(20), L20604. <https://doi.org/10.1029/2012GL053717>
- Hobday, A. J., Alexander, L. V., Perkins, S. E., Smale, D. A., Straub, S. C., Oliver, E. C. J., et al. (2016). A hierarchical approach to defining marine heatwaves. *Progress in Oceanography*, 141, 227–238.
- Hogg, N. G., & Stommel, H. (1985). On the relation between the deep circulation and the Gulf Stream. *Deep sea research Part A. Oceanographic Research Papers*, 32(10), 1181–1193. [https://doi.org/10.1016/0198-0149\(85\)90002-0](https://doi.org/10.1016/0198-0149(85)90002-0)
- Holland, W. R. (1978). The role of mesoscale eddies in the general circulation of the ocean—Numerical experiments using a wind-driven quasi-geostrophic model. *Journal of Physical Oceanography*, 8(3), 363–392. [https://doi.org/10.1175/1520-0485\(1978\)008<0363:tromei>2.0.co;2](https://doi.org/10.1175/1520-0485(1978)008<0363:tromei>2.0.co;2)
- Holland, W. R., & Lin, L. B. (1975). On the generation of mesoscale eddies and their contribution to the Oceanic General circulation. II. A parameter study. *Journal of Physical Oceanography*, 5(4), 658–669. [https://doi.org/10.1175/1520-0485\(1975\)005<0658:otgome>2.0.co;2](https://doi.org/10.1175/1520-0485(1975)005<0658:otgome>2.0.co;2)
- Hu, Z. Y., Petrenko, A. A., Doglioli, A. M., & Dekeyser, I. (2011). Numerical study of eddy generation in the western part of the Gulf of Lion. *Journal of Geophysical Research*, 116(C12). <https://doi.org/10.1029/2011jc007074>
- Ioannou, A., Stegner, A., Dubos, T., Le Vu, B., & Speich, S. (2020). Generation and intensification of mesoscale anticyclones by orographic wind jets: The case of Ierapetra eddies forced by the Etesians. *Journal of Geophysical Research: Oceans*, 125(8), e2019JC015810. <https://doi.org/10.1029/2019jc015810>
- Ioannou, A., Stegner, A., Dumas, F., & Le Vu, B. (2020). Three-dimensional evolution of mesoscale anticyclones in the lee of Crete. *Frontiers in Marine Science*, 7, 1019. <https://doi.org/10.3389/fmars.2020.609156>
- Isern-Fontanet, J., Font, J., García-Ladona, E., Emelianov, M., Millot, C., & Taupier-Letage, I. (2004). Spatial structure of anticyclonic eddies in the Algerian basin (Mediterranean Sea) analyzed using the Okubo–Weiss parameter. *Deep Sea Research Part II: Topical Studies in Oceanography*, 51(25–26), 3009–3028. <https://doi.org/10.1016/j.dsr2.2004.09.013>
- Jansà, A. (1987). Distribution of the mistral: A satellite observation. *Meteorology and Atmospheric Physics*, 36, 201–214.
- Jouanno, J., Sheinbaum, J., Barnier, B., & Molines, J.-M. (2009). The mesoscale variability in the Caribbean Sea. Part II: Energy sources. *Ocean Modelling*, 26(3), 226–239. <https://doi.org/10.1016/j.ocemod.2008.10.006>
- Juza, M., Escudier, R., Pascual, A., Pujol, M.-I., Taburet, G., Troupin, C., et al. (2016b). Impacts of reprocessed altimetry on the surface circulation and variability of the Western Alboran Gyre. *Advances in Space Research*. <https://doi.org/10.1016/j.asr.2016.05.026>
- Juza, M., Escudier, R., Vargas-Yáñez, M., Mourre, B., Heslop, E., Allen, J., & Tintoré, J. (2019). Characterization of changes in Western Intermediate Water properties enabled by an innovative geometry-based detection approach. *Journal of Marine Systems*, 191, 1–12. <https://doi.org/10.1016/j.jmarsys.2018.11.003>
- Juza, M., Mourre, B., Renault, L., Gómara, S., Sebastián, K., Lora, S., et al. (2016). SOCIB operational ocean forecasting system and multi-platform validation in the Western Mediterranean Sea. *Journal of Operational Oceanography*, 9(sup1), S155–S166. <https://doi.org/10.1080/175876X.2015.1117764>
- Kahru, M., Mitchell, B. G., Gille, S. T., Hewes, C. D., & Holm-Hansen, O. (2007). Eddies enhance biological production in the Weddell-Scotia confluence of the Southern Ocean. *Geophysical Research Letters*, 34(14). <https://doi.org/10.1029/2007GL030430>
- Kang, D., & Curchitser, E. N. (2015). Energetics of eddy–mean flow interactions in the Gulf Stream region. *Journal of Physical Oceanography*, 45(4), 1103–1120. <https://doi.org/10.1175/JPO-D-14-0200.1>
- Krom, M. D., Brenner, S., Kress, N., Neori, A., & Gordon, L. I. (1992). Nutrient dynamics and new production in a warm-core eddy from the eastern Mediterranean Sea. *Deep sea research Part A. Oceanographic Research Papers*, 39(3), 467–480. [https://doi.org/10.1016/0198-0149\(92\)90083-6](https://doi.org/10.1016/0198-0149(92)90083-6)
- Lobel, P. S., & Robinson, A. R. (1986). Transport and entrainment of fish larvae by ocean mesoscale eddies and currents in Hawaiian waters. *Deep Sea Research Part A. Oceanographic Research Papers*, 33(4), 483–500. [https://doi.org/10.1016/0198-0149\(86\)90127-5](https://doi.org/10.1016/0198-0149(86)90127-5)
- López-García, M. J., Millot, C., Font, J., & García-Ladona, E. (1994). Surface circulation variability in the Balearic Basin. *Journal of Geophysical Research*, 99(C2), 3285–3296. <https://doi.org/10.1029/93JC02114>
- Mahadevan, A., & Archer, D. (2000). Modeling the impact of fronts and mesoscale circulation on the nutrient supply and biogeochemistry of the upper ocean. *Journal of Geophysical Research*, 105(C1), 1209–1225. <https://doi.org/10.1029/1999JC900216>
- Marbà, N., & Duarte, C. M. (2010). Mediterranean warming triggers seagrass (*Posidonia oceanica*) shoot mortality. *Global Change Biology*, 16(8), 2366–2375. <https://doi.org/10.1111/j.1365-2486.2009.02130.x>
- Marshall, J. C. (2006). Eddy-mean-flow interaction in a barotropic ocean model. *Quarterly Journal of the Royal Meteorological Society*, 110(465), 573–590. <https://doi.org/10.1002/qj.49711046502>
- Mason, E., & Pascual, A. (2013). Multiscale variability in the Balearic Sea: An altimetric perspective. *Journal of Geophysical Research: Oceans*, 118(6), 3007–3025. <https://doi.org/10.1002/jgrc.20234>
- Millot, C. (1999). Circulation in the Western Mediterranean Sea. *Journal of Marine Systems*, 20(1), 423–442. [https://doi.org/10.1016/S0924-7963\(98\)00078-5](https://doi.org/10.1016/S0924-7963(98)00078-5)

- Millot, C., & Taupier-Letage, I. (2005). Circulation in the Mediterranean Sea. In *The Mediterranean Sea* (pp. 29–66). Springer. <https://doi.org/10.1007/b107143>
- Mourre, B., Aguiar, E., Juza, M., Hernandez-Lasheras, J., Reyes, E., Heslop, E., et al. (2018). Assessment of high-resolution Regional Ocean prediction systems using multi-platform observations: Illustrations in the Western Mediterranean Sea. In *New Frontiers in Operational Oceanography* (Vol. 663–694). GODAE Ocean View. <https://doi.org/10.17125/gov2018>
- Nagai, T., Gruber, N., Frenzel, H., Lachkar, Z., McWilliams, J. C., & Plattner, G.-K. (2015). Dominant role of eddies and filaments in the offshore transport of carbon and nutrients in the California Current System. *Journal of Geophysical Research: Oceans*, 120(8), 5318–5341. <https://doi.org/10.1002/2015JC010889>
- Okubo, A. (1970). Horizontal dispersion of floatable particles in the vicinity of velocity singularities such as convergences. *Deep-Sea Research and Oceanographic Abstracts*, 17(3), 445–454. [https://doi.org/10.1016/0011-7471\(70\)90059-8](https://doi.org/10.1016/0011-7471(70)90059-8)
- Onken, R., Álvarez, A., Fernández, V., Vizoso, G., Basterretxea, G., Tintoré, J., et al. (2008). A forecast experiment in the Balearic Sea. *Journal of Marine Systems*, 71(1), 79–98. <https://doi.org/10.1016/j.jmarsys.2007.05.008>
- Parravicini, V., Guidetti, P., Morri, C., Montefalcone, M., Donato, M., & Bianchi, C. N. (2010). Consequences of sea water temperature anomalies on a Mediterranean submarine cave ecosystem. *Estuarine, Coastal and Shelf Science*, 86(2), 276–282. <https://doi.org/10.1016/j.ecss.2009.11.004>
- Pascual, A., Buongiorno, N. B., Larnicol, G., Emelianov, M., & Gomis, D. (2002). A case of an intense anticyclonic eddy in the Balearic Sea (western Mediterranean). *Journal of Geophysical Research*, 107(C11), 4–1. <https://doi.org/10.1029/2001jc000913>
- Pedlosky, J. (1982). Quasigeostrophic motion of a stratified fluid on a sphere. In *Geophysical fluid dynamics* (pp. 314–422). Springer. [https://doi.org/10.1007/978-3-662-25730-2\\_6](https://doi.org/10.1007/978-3-662-25730-2_6)
- Peng, Q., Xie, S. P., Wang, D., Zheng, X. T., & Zhang, H. (2019). Coupled ocean-atmosphere dynamics of the 2017 extreme coastal El Niño. *Nature Communications*, 10(1), 1–10. <https://doi.org/10.1038/s41467-018-08258-8>
- Pérez, T., Garrabou, J., Sartoretto, S., Harmelin, J.-G., Francour, P., & Vacelet, J. (2000). Mortalité massive d'invertébrés marins: Un événement sans précédent en méditerranée nord-occidentale. *Comptes Rendus de l'Académie des Sciences - Series III: Sciences de la Vie*, 323(10), 853–865.
- Pessini, F., Olita, A., Cotroneo, Y., & Perilli, A. (2018). Mesoscale eddies in the Algerian Basin: Do they differ as a function of their formation site? *Ocean Science*, 14(4), 669–688. <https://doi.org/10.5194/os-14-669-2018>
- Poulain, P. M., Menna, M., & Mauri, E. (2012). Surface geostrophic circulation of the Mediterranean Sea derived from drifter and satellite altimeter data. *Journal of Physical Oceanography*, 42(6), 973–990. <https://doi.org/10.1175/jpo-d-11-0159.1>
- Prieto, L., Macías, D., Peliz, A., & Ruiz, J. (2015). Portuguese Man-of-War (*Physalia physalis*) in the Mediterranean: A permanent invasion or a casual appearance? *Scientific Reports*, 5(1), 1–7. <https://doi.org/10.1038/srep11545>
- Pujol, M. I., & Larnicol, G. (2005). Mediterranean sea eddy kinetic energy variability from 11 years of altimetric data. *Journal of Marine Systems*, 58(3–4), 121–142. <https://doi.org/10.1016/j.jmarsys.2005.07.005>
- Rubio, A., Arnau, P. A., Espino, M., Flexasdel, M. M., Jordà, G., Salat, J., et al. (2005). A field study of the behaviour of an anticyclonic eddy on the Catalan continental shelf (NW Mediterranean). *Progress in Oceanography*, 66(2), 142–156. <https://doi.org/10.1016/j.poccean.2004.07.012>
- Rubio, A., Barnier, B., Jordà, G., Espino, M., & Marsaleix, P. (2009). Origin and dynamics of mesoscale eddies in the Catalan Sea (NW Mediterranean): Insight from a numerical model study. *Journal of Geophysical Research*, 114(C6). <https://doi.org/10.1029/2007JC004245>
- Rypina, I. I., Pratt, L. J., Entner, S., Anderson, A., & Cherian, D. (2020). The influence of an eddy in the success rates and distributions of passively advected or actively swimming biological organisms crossing the continental slope. *Journal of Physical Oceanography*, 50(7), 1839–1852. <https://doi.org/10.1175/jpo-d-19-0209.1>
- Sabatés, A., Salat, J., Palomera, I., Emelianov, M., Fernández de Puelles, M. L., & Olivar, M. P. (2007). Advection of anchovy (*Engraulis encrasicolus*) larvae along the Catalan continental slope (NW Mediterranean). *Fisheries Oceanography*, 16(2), 130–141. <https://doi.org/10.1111/j.1365-2419.2006.00416.x>
- Sabatés, A., Salat, J., Raya, V., & Emelianov, M. (2013). Role of mesoscale eddies in shaping the spatial distribution of the coexisting *Engraulis encrasicolus* and *Sardinella aurita* larvae in the northwestern Mediterranean. *Journal of Marine Systems*, 111, 108–119. <https://doi.org/10.1016/j.jmarsys.2012.10.002>
- Salihoglu, İ., Saydam, C., Baştürk, Ö., Yılmaz, K., Göçmen, D., Hatipoğlu, E., & Yılmaz, A. (1990). Transport and distribution of nutrients and chlorophyll-a by mesoscale eddies in the northeastern Mediterranean. *Marine Chemistry*, 29, 375–390. [https://doi.org/10.1016/0304-4203\(90\)90024-7](https://doi.org/10.1016/0304-4203(90)90024-7)
- Shchepetkin, A. F., & McWilliams, J. C. (2005). The regional oceanic modeling system (ROMS): Split-explicit, free-surface, topography-following-coordinate oceanic model. *Ocean Modelling*, 9(4), 347–404. <https://doi.org/10.1016/j.ocemod.2004.08.002>
- Siegel, D. A., Peterson, P., McGillicuddy, D. J., Jr, Maritorena, S., & Nelson, N. B. (2011). Bio-optical footprints created by mesoscale eddies in the Sargasso Sea. *Geophysical Research Letters*, 38(13). <https://doi.org/10.1029/2011GL047660>
- Simoncelli, S., Fratianni, C., Pinardi, N., Grandi, A., Drudi, M., Oddo, P., & Dobricic, S. (2019). Mediterranean Sea physical Reanalysis (CMEMS MED-physics) [Data set]. Copernicus Monitoring Environment Marine Service (CMEMS). [https://doi.org/10.25423/MEDSEA\\_REANALYSIS\\_PHYS\\_006\\_004](https://doi.org/10.25423/MEDSEA_REANALYSIS_PHYS_006_004)
- Small, R. J., deSzoeke, S. P., Xie, S. P., O'Neill, L., Seo, H., Song, Q., et al. (2008). Air–sea interaction over ocean fronts and eddies. *Oceanic Fronts*, 45(3), 274–319. <https://doi.org/10.1016/j.dynatmoe.2008.01.001>
- Storch, J.-S. V., Eden, C., Fast, I., Haak, H., Hernández-Deckers, D., Maier-Reimer, E., et al. (2012). An estimate of the Lorenz energy cycle for the world ocean based on the STORM/NCEP simulation. *Journal of Physical Oceanography*, 42(12), 2185–2205. <https://doi.org/10.1175/JPO-D-12-079.1>
- Taupier-Letage, I., Puillat, I., Millot, C., & Raimbault, P. (2003). Biological response to mesoscale eddies in the Algerian Basin. *Journal of Geophysical Research*, 108(C8). <https://doi.org/10.1029/1999JC000117>
- Tintoré, J., Pinardi, N., Álvarez-Fanjul, E., Aguiar, E., Álvarez-Berastegui, D., Bajo, M., et al. (2019). Challenges for sustained observing and forecasting systems in the Mediterranean Sea. *Frontiers in Marine Science*, 6, 568. <https://doi.org/10.3389/fmars.2019.00568>
- Tintoré, J., Vizoso, G., Casas, B., Heslop, E., Pascual, A., Orfila, A., et al. (2013). SOCIB: The Balearic Islands coastal ocean observing and forecasting system responding to science, technology and society needs. *Marine Technology Society Journal*, 47(1), 101–117.
- Tintoré, J., Wang, D.-P., & La Violette, P. E. (1990). Eddies and thermohaline intrusions of the shelf/slope front off the northeast Spanish coast. *Journal of Geophysical Research*, 95(C2), 1627–1633. <https://doi.org/10.1029/JC095IC02p01627>
- Undén, P., Rontu, L., Järvinen, H., Lynch, P., Calvo, J., Cats, G., et al. (2002). *HIRLAM-5 scientific documentation*.
- Wang, Y., Zhang, H.-R., Chai, F., & Yuan, Y. (2018). Impact of mesoscale eddies on chlorophyll variability off the coast of Chile. *PLoS One*, 13(9), e0203598. <https://doi.org/10.1371/journal.pone.0203598>



- Weiss, J. (1991). The dynamics of enstrophy transfer in two-dimensional hydrodynamics. *Physica D: Nonlinear Phenomena*, 48(2), 273–294. [https://doi.org/10.1016/0167-2789\(91\)90088-Q](https://doi.org/10.1016/0167-2789(91)90088-Q)
- Xie, L., Liu, X., & Pietrafesa, L. J. (2007). Effect of bathymetric curvature on Gulf Stream instability in the vicinity of the Charleston Bump. *Journal of Physical Oceanography*, 37(3), 452–475. <https://doi.org/10.1175/JPO2995.1>
- Zhan, P., Subramanian, A. C., Yao, F., Kartadikaria, A. R., Guo, D., & Hoteit, I. (2016). The eddy kinetic energy budget in the Red Sea. *Journal of Geophysical Research: Oceans*, 121(7), 4732–4747. <https://doi.org/10.1002/2015JC011589>
- Zhang, Z., Wang, W., & Qiu, B. (2014). Oceanic mass transport by mesoscale eddies. *Science*, 345(6194), 322–324. <https://doi.org/10.1126/science.1252418>